Low Frequency Modeling and Experimental Validation of Passive Noise Attenuation in Ear Defenders

by

Jonathan D. Sides

Thesis submitted to the Faculty of the Virginia Polytechnic Institute and State University in partial fulfillment of the requirements for the degree of

MASTERS OF SCIENCE IN MECHANICAL ENGINEERING

William R. Saunders, Chair

Ricardo A. Burdisso

Robert L.West

June 10, 2004

Blacksburg, Virginia

Keywords (Noise, attenuation, passive, ear, defender, frequency)

Low Frequency Modeling and Experimental Validation of Passive Noise Attenuation in Ear Defenders

by

Jonathan D. Sides

William R. Saunders, Chairman

Department of Mechanical Engineering

(ABSTRACT)

Circumaural ear cups have been used for decades as an effective way of protecting users from high noise fields. Over the decades, a number of researchers dedicated their time to understanding the dynamics that govern the attenuation of hearing protectors. This thesis duplicates some of this work with newer technology and better data processing ability. In addition to revitalizing the accepted knowledge of hearing protector technology, this thesis is the first documented effort to show how the previously ignored air leak, known to exist between the ear cup and the head, has a profound effect on the low and mid frequency attenuation of a circumaural hearing defender.

Past research focused on the mechanical vibration of the cup on the seal as the main source of noise within the ear cup. This mechanical vibration, known as the piston resonance exists, and affected noise attenuation within the ear cup. A reasonably sized air leak of 160 e^{-7} m^2 however, overwhelmed the piston resonance. An air leak of this size was shown to degrade noise attenuation by over 50 dB at 40Hz and 30 dB at 200 Hz when compared to a no-leak case. Further testing also suggested that the air leak has the ability to continue adding energy into the cup up to 3000 Hz.

To

Sarah

Acknowledgements

There are so many people to thank, well, actually, just a few. First, thanks to Dr. Saunders, who gave me the opportunity to do this research. Without his help and guidance I don't think I could have gotten through. My fiancée Sarah has been exceptionally supportive, allowing me to work on my thesis by taking care of chores around the house. Without her, I'm pretty sure we wouldn't get our security deposit back. My parents did their part. They always kept me fed and encouraged when things looked grim. Finally, how can I forget Losh, the man who barely acknowledged me in his acknowledgements. He helped me get through the nitty gritty problems that thesis writing can create. He also has a great lake house. Thank you everyone.

Table of Contents

List of Figures

List of Tables

1 Introduction

For decades, circumaural ear cups have been implemented as an effective form of passive noise attenuation in high noise fields. During this time, a handful of researchers have dedicated time to modeling and experimentally validating the dynamics that control noise attenuation in these hearing defenders. Much of the research conducted took place during the middle of the twentieth century, before much of the currently used acoustic instrumentation was available. Today, noise fields are increasing, and current hearing defenders are incapable of passively attenuating these higher noise fields to a safe level for the user. This issue is causing concern for the NAVY. The noise field that will be created by the new Joint Strike Fighter will pose a threat to the hearing health of the naval ground crew that services these aircraft. For this reason, the NAVY has taken an interest in providing more adequate hearing protection for their personnel.

Currently, flight deck crews exposed to high noise fields use dual hearing protection. This protection consists of foam earplugs and circumaural ear cups. It is currently accepted that this combination of passive hearing protection has an attenuation limit, but there has been no consensus on what the limit is. Of the hearing protection methods, personal passive hearing protectors are the most inexpensive, and widely distributed. Despite this, there has been no recent documented effort to understand the dynamics controlling the passive noise attenuation limits of a circumaural ear cup. In an effort to find adequate hearing protection for their personnel, the NAVY has invested in research to model and experimentally validate the dynamics that govern the passive noise attenuation of circumaural hearing defenders.

An effective ear defender must protect the user from a wide frequency range of noise. Across this range are multitudes of physical mechanisms that control the attenuation of the ear defender. Many of these mechanisms can be identified within the frequency range they are most dominant in. The goal of this research is to model and experimentally validate the mechanisms that control ear cup noise attenuation below 800Hz. The secondary goal of this research is to measure the mid frequency response of the ear cup and look at factors that may affect noise attenuation in this range.

There are many physical mechanisms to consider when modeling the low frequency (below 800 Hz) dynamics of the ear cup. Transmission loss through the ear cup and seal material is generally the first thing to consider. Noise can also be transmitted to the eardrum through bone conduction. This is also referred to as body conduction. Another physical mechanism to consider is the mechanical resonance of the ear cup on the seal. This is referred to as the piston resonance. Many early researchers, such as Shaw, believed that the piston resonance was responsible for the low frequency response of the ear cup. The final low frequency mechanism to consider is an acoustic resonance introduced to the ear cup by an imperfect seal formed between the ear cup and the head. This is known as the Helmholtz resonance. There is recent literature that focuses on transmission loss of materials and bone conduction, thus, these two topics are not discussed in this document.

1.1 Organization of Thesis

This thesis document is broken into two major sections. The low frequency modeling is covered in the first half of the document. The experimental validation of these models is covered in the second half of the document. In addition to these sections, a literature review is presented to give the reader an idea of how this research fits in with past work in the field of passive noise attenuation. Finally, the conclusion highlights the results of the research as well as suggests ideas for future work.

A review of the existing literature written about hearing protection provides an insight to the commonly accepted mechanisms that control passive hearing attenuation in ear cups. The bulk of this research was conducted in the middle of the twentieth century. Later research focused on the attenuation limits of a hearing protector. After sorting through this research, it becomes clear that the current understanding of circumaural hearing protection is incomplete. To constructively add to this knowledge base, it is necessary to model and experimentally validate the physical mechanisms that control passive noise attenuation in circumaural hearing protectors.

The modeling section of this document presents the analytical models of the physical mechanisms acting on the ear cup. The Helmholtz resonance and piston resonance are modeled using single degree of freedom spring-mass-damper analysis. This analysis is extended to a coupled model of these two phenomena. The last model

highlighted in this chapter is the velocity of the air within the Helmholtz duct. Parallel research is also being conducted to model these dynamics with FEA (Finite Elements Analysis).

The testing section covers the experimental validation of the analytical models described in the modeling section. The mid-frequency acoustic mode shapes are identified and compared with FEA results. Testing was also extended to examine the effects of a foam insert on the frequency response of the ear cup.

2 Literature Review

Passive hearing protection has not been an important area of research for many years. The limited number of papers written on the subject is evidence of this. This chapter provides a comprehensive review of the previous research done on head set noise attenuation. This review will also make evident the fact that the air leak has been ignored and/or dismissed as a significant contributor of noise. This chapter will summarize the previous work in chronological order.

2.1 [Von Gierke et al. 1953]

Von Gierke was interested in the limits of hearing protection. He set out to find the maximum attenuation that could be achieved with hearing defenders. Von Gierke recognized that even with a perfect ear defender, noise would still be transmitted through the body to the ear. The test method then became to completely occlude the ear so that the ambient sound field transmits no sound, but instead by the sound conducted by the bone and tissue. He proposed that this would be the theoretical limit of all types of hearing protectors.

Von Gierke conducted a number of tests to determine the limits of hearing attenuation. To do this, he spent a great amount of time covering the ear, and exciting different body parts with noise. He stated "Great care was taken to assure that the sound to which the observer responded entered by way of the forehead and not through the auditory canal in spite of the earplug". The care taken for the forehead tests was also taken with the other tests. These tests were taken on the sternum, forehead and abdomen. In these tests, Von Gierke states that the hearing protection only accounted for 12 dB of noise attenuation. The conclusion of the paper was that below 500 Hz, the maximum attenuation that could be achieved was 28 dB. Above this frequency, the best attenuation would be between 40 and 50 dB. The poor attenuation at low frequencies was attributed to the mechanical resonance of the earplug.

2.2 [Shaw et al. 1958]

Shaw was interested in understanding the physics of low frequency attenuation. It was his contention that "…sound reaches the ear through well-fitting ear defenders by setting the whole ear defender into vibration". Shaw initially analyzed the problem by using a simple spring mass damper system. From this model, he was able to design a cup that would provide better attenuation.

Shaw did recognize that a nearly airtight seal was necessary. He also noted that using a soft sponge seal was detrimental to low frequency performance. Shaw replaced the soft sponge seal with a liquid filled cushion. This seal worked very well, but he then realized that the flesh set the spring constant limit. Even if the seal was perfectly stiff, the flesh still had compliance, and thus the flesh sets the limit to the attenuation that may be achieved with the defenders.

2.3 [Thiessen et al. 1962]

Until the time of this paper, very little research had been done investigating the effects of placing a speaker within a hearing protection device. Thiessen noted that the requirements of minimum sound transmission and maximum earphone sensitivity are partially incompatible. Thiessen then looks at this problem with a single cavity and dual cavity model. He then concludes that the best system is the dual cavity configuration. This configuration allows for strong coupling between the two cavities at low frequencies, and poor coupling at high frequencies. This allows the effective volume that the ear "sees" to be larger at low frequencies, and smaller at high frequencies. This increases the sensitivity of the earphone, and increases attenuation. Thiessen was able to show that the dual cavity ear cup has a constant response over a large frequency range. This was shown through models and experimental data.

2.4 [Goff et al. 1984]

Goff was interested in testing hearing protection devices for the mining industry. This industry is comprised of personnel that work in high noise fields for extended periods of time. Goff fitted 45 workers with earmuffs for the purpose of testing the actual noise attenuation seen in the field. Goff placed two microphones on each of the

test subjects; one next to the ear canal and the other on the corresponding shoulder. Time data of the microphones was then recorded on a dual track tape recorder for an extended period of time. Goff noted that better attenuation was achieved at higher frequencies (above 2000 Hz). He also noted that the actual noise attenuation seen in the field was lower than predicted by NIOSH and ANSI. Goff also saw an amplification of noise between 80 and 315 Hz.

2.5 [Pääkkönen et al. 1992]

Pääkkönen set out to examine the effects of different variables on the noise attenuation of an earmuff. Pääkkönen conducted a number of different tests in an anechoic room, a low frequency chamber and with an acoustic test fixture in an acoustic tunnel. The results of these tests showed that changes in the cup and foam lining improved attenuation as much as 10 dB, and changes in the dynamic stiffness and damping of the cushion improved attenuation as much as 4 dB. These changes in attenuation were seen primarily above 1000 Hz. Below 1000 Hz, the most effective parameters in noise attenuation were the cup volume, and the headband force exerted on the cup. The spring force also had noticeable effects above 3000 Hz. It was also noted that breaks in the cushion, or holes in the cup deteriorated noise attenuation by as much as 30 dB. Pääkkönen concluded that a tight fitting between the skin and cushion, an increase of headband force and an increase of absorption within the cup improved the attenuation of the ear cup.

2.6 [Rimmer et al. 1997]

In this journal article, Rimmer proposes a new method of noise attenuation measurement for hearing protection devices (HPD). Rimmer proposes a method called BCLB (bone conduction loudness balance). This test is intended to nullify the effect of not being able to test REAT (Real Ear Attenuation) in a 0-dB environment. Comparing a variable sound level to a known sound level does this. He used pure tones and noise bands. He used a third octave noise band centered at 2000 Hz in order to nullify the effect bone conduction at the lower frequencies. It is Rimmer's contention that bone

conduction has the largest effects at lower frequencies. Rimmer also mentions that HPD's are less effective below 2000 Hz.

This journal article comes back to a concept discussed earlier. The effects of bone conduction may be a limiting factor in the low frequency attenuation of HPD's. Rimmer set out to test his new method of hearing protection measurement. He used 4 subjects with no prior experience using hearing protection. Rimmer's results showed a 0-4 dB difference between REAT testing and his new method, BCLB.

2.7 [Gauger et al. 2003]

In this journal article, Gauger sets out to find the maximum hearing protection that can be achieved with conventional hearing protection devices. Military personnel exposed to 150 dB sound fields motivate Gauger's research. The tests conducted for this paper used double hearing protection. A longer, 24 mm earplug was used in conjunction with a Gentex fighter/attack aircrew helmet (HGU-84/P). Gauger used 16 test subjects, of which fourteen of them met the ANSI S12.6-1997 hearing requirements. The other two test subjects met the requirements at all but one frequency. Both the helmet and the earplugs were fitted to achieve ideal noise protection. Testing was conducted from 125 Hz to 8 kHz using 1/3 octave bands.

Maximum attenuation attainable is higher than previously predicted. Gauger shows that maximum attenuation is around 40 to 60 dB. Low frequency noise attenuation was shown to be better than previously predicted by Von Gierke. This paper also assumes a perfect seal, and that no air makes it to the ear canal. Gauger was also able to show that attenuation could approach the limits of bone conduction above 2000 Hz. Gauger is able to achieve 51 dB of noise attenuation after 2000 Hz, but only 41 dB of attenuation below 2000 Hz. Gauger does not approach the bone conduction limits at low frequencies, and no mention was made of the reason for this.

2.8 [Birch et al. 2003]

This paper examines the effectiveness of hearing protectors in a high amplitude impulse noise field. Birch designed an acoustic test fixture for the evaluation of hearing protection devices in this kind of sound field. The acoustic test fixture, referred to as

ATF, consisted of a high-pressure generator, and a long tube. The system was capable of producing noise levels as high as 160 dB SPL. Birch concluded that the ATF could be used to measure HPD attenuation up to 45 dB, but little testing of the HPD was actually conducted.

2.9 [Hsu et al. 2004]

Hsu wrote this paper to help improve the comfort of hearing protectors so as to increase the willingness of the workers to wear HPD's. Hsu began this work by finding the comfort needs of workers through a questionnaire. The result of this questioning was the "comfort indices" from which a comfort tester was designed. The comfort tester simultaneously measures the air-tightness, heat conduction ability and the headband force of an earmuff. Hsu concluded that a headband force should not be much higher than 10.5 Newtons. He also noted that earmuffs with larger interior volumes tend to have a lower interior temperature.

2.10 [Casali et al. 2004]

The research in this paper was conducted for the purposes of gaining useful estimates of HPD field performance. In the tests, experimenter-fit, informed-user-fit, and subject-fit methods were used. The subject-fit method depends on listeners who are audio metrically proficient, but inexperienced in the use of hearing protection devices. It was found that the subject-fit method produced the most consistent results between the labs. Through this research, formulas were created to determine the minimum detectable difference between attenuation. These formulas also are able to determine the minimum number of test subjects to achieve that level of precision. "For a precision of 6 dB, the study found that the minimum number of subjects was 4 for the Bilsom UF-1 earmuff, 10 for the E.A.R. Classic earplug, 31 for the Willson EP100 earplug, and 22 for the PlasMed V-51R earplug."

2.11 Literature Review Summary

A review of the existing literature written about hearing protection provides an insight to the commonly accepted mechanisms that control passive hearing attenuation in ear cups. The bulk of this research was conducted in the middle of the twentieth century. Later research focused on the attenuation limits of a hearing protector. After sorting through this research, it becomes clear that the current understanding of circumaural hearing protection is incomplete. To constructively add to this knowledge base, it is necessary to model and experimentally validate the physical mechanisms that control passive noise attenuation in circumaural hearing protectors.

3 Modeling

The David Clark Company Inc. (DCCI) 9AN/2 is a circumaural hearing protection device. The purpose of a hearing protection device is to attenuate ambient noise levels to a safe sound pressure level for the user. The DCCI ear cup implements a rigid cup, soft seal, and stiff headband to accomplish this goal.

Figure 3.1: DCCI 9AN/2 ear cup with DCCI undercut seals

Figure 3.1 shows the DCCI hearing protection device in its mounted position. The black seals shown are aftermarket gel seals sold by David Clark Company.

The goal of the ear cup modeling in this chapter is to analytically represent the low frequency dynamics that occur within an ear cup. These analytical models will be compared to test results, and then to FEA models.

3.1 Helmholtz Resonator

Nearly all circumaural hearing protectors form an imperfect seal around the ear. Imperfect sealing introduces air leaks to the inner cavity of the ear cup from the ambient. These leaks, in conjunction with the ear cup, facilitate a phenomenon known as the

Helmholtz resonance. The Helmholtz resonance is a well-documented phenomenon that occurs when a slug of fluid oscillates between a rigid walled volume and the ambient surroundings. This dynamic occurs when the fluid in the leak responds in bulk. A bulk response is defined as spatially uniform fluid motion that occurs at low frequencies when λ (wavelength)>>L (length of the leak), $\lambda >> \forall^{1/3}$(volume of cup), and $\lambda >> A_l^{1/2}$(leak area). A single order of magnitude is considered "much greater than", and as such the bulk fluid assumption is valid for all these parameters up until 2700 Hz for the DCCI 9AN/2 ear cup.

The Helmholtz resonator is modeled as a spring-mass-damper system. The seal for this model is assumed to be rigid. The fluid in the leak represents the mass. The compression within the rigid volume provides stiffness. The open end of the neck radiates sound, introducing a radiation resistance. The fluid moving within the leak introduces a thermoviscous resistance.

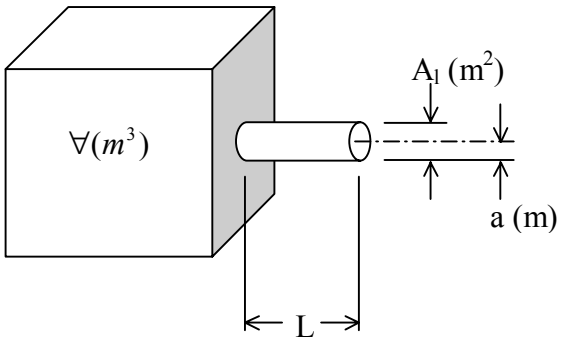

Figure 3.2: The simple Helmholtz resonator

Figure 3.2 illustrates a schematic of a Helmholtz resonator. When the system is at rest, the slug of fluid is contained within the length L. The viscous losses are a function of this length, as well as the area of the leak, A_l. The volume,$\forall$, is used to evaluate the stiffness of the system. Using basic vibration techniques leads to a single degree of freedom spring-mass-damper system.

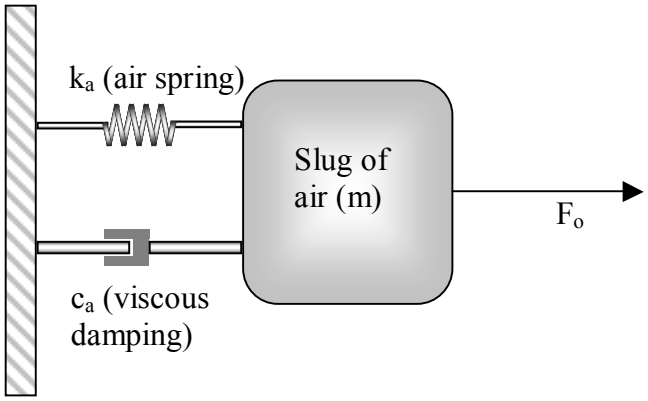

Figure 3.3: Spring-mass-damper system of the Helmholtz resonator

Figure 3.3 is a spring-mass-damper representation of the Helmholtz resonator. An analysis of this system begins with a free body diagram. This is the first step in deriving a force balance equation. Figure 3.4 represents the free body diagram of the system.

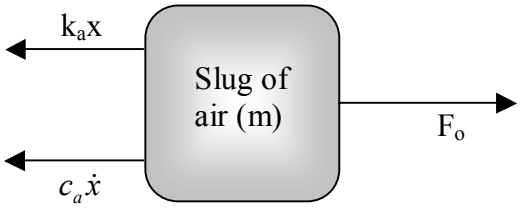

Figure 3.4: Free body diagram of the Helmholtz resonator

The force, F_o, is a function of an outside pressure source. The pressure, P_o, acts over the area of the leak (A_l). Variables will be defined as they appear in equations. The first equation, derived from the free body diagram in Figure 3.4, is the equation of motion.

$$m\ddot{x} + c_a\dot{x} + k_a x = F_o$$

Equation 3-1

Equation 3-1 is used to model the resonator. The coefficients, m, c_a, and k_a are functions of physical parameters. These coefficients are defined as (Kinsler and Frey, 2000):

$$m = \rho_o A_l L' \quad (kg)$$

Equation 3-2

$$L' = L + 1.4a \quad (m)$$

Equation 3-3

m = mass of air in leak (kg)
L' = effective leak length (m)
ρ_o = density of air (kg/m^3)
A_l = surface area of leak (m^2)
L = length of leak (m)

The only variable that has not been previously introduced is L'. This variable is an effective leak length that is used to compensate for the effects of fluid momentum. As the slug of fluid is accelerated through the leak, it does not lose its momentum at the end of the leak. The momentum of the fluid dissipates over some length past the leak. This length, in addition to the physical leak length, comprises the effective leak length.

The damping term, c_a, is composed of two terms, radiation resistance and thermoviscous resistance. The radiation resistance is a representation of losses due to sound radiation into the open medium outside the leak. This component of the damping term is represented as R_r (Kinsler and Frey, 2000).

$$R_r = \frac{\rho_o c k^2 A_l^2}{4\pi} \quad \left(\frac{kg}{s}\right)$$

Equation 3-4

R_r = radiation resistance (kg/s)
c = speed of sound in air at STP (m/s)
k = wavenumber (1/m)

The second component of the damping term is the thermoviscous resistance. This term represents the losses due to viscous boundary layer effects at or near the wall. The thermoviscous resistance, R_w is represented below (Kinsler and Frey, 2000).

$$R_w = 2mc\alpha_w \quad \left(\frac{kg}{s}\right)$$

Equation 3-5

where α_w (1/m) is the absorption coefficient and is defined as (Kinsler and Frey, 2000):

$$\alpha_w = \frac{1}{ac}\left(\frac{\eta\omega}{2\rho_o}\right)^{1/2}\left(1+\frac{\gamma-1}{\sqrt{\Pr}}\right) \qquad \left(\frac{1}{m}\right)$$

$$\eta = \frac{1}{3}\rho_o l_m c \qquad \left(\frac{N\cdot s}{m^2}\right)$$

Equation 3-6

where:

η = viscosity ($N*s/m^2$)
ω = frequency (1/s)
γ = specific heat ratio
Pr = Prandtl number
l_m = mean free path between atoms (m)

The viscosity can be calculated, but it is convenient to use a tested value of 184×10^{-7} ($N*s/m^2$) (Schetz, 513). The sum of the resistance terms yields the total resistance of the system such that $c_a = (R_r+R_w)$. For now, this term is an estimate that will have to be calibrated during testing.

The final term to define is the stiffness. In a normal spring-mass-damper system, the stiffness is represented by a mechanical spring. The stiffness of the air spring is a function of the internal pressure of the cup. The internal pressure of the cup is below (Kinsler and Frey, 2000).

$$P_i = \frac{\rho_o c^2 A_l}{\forall_{cup}} x \qquad (Pa)$$

Equation 3-7

Seen in Equation 3-7, the internal pressure of the cup is a function of the volume ($\forall$) of the cup, the leak area (A_l) and the distance the slug of fluid travels (x). It is also a function of the density and speed of sound of air. The stiffness of the air spring is found using a simple relationship.

$$k_a = \frac{P_i A_l}{x} \qquad \left(\frac{N}{m}\right)$$

Equation 3-8

Substituting Equation 3-7 into Equation 3-8, an expression for the air spring is obtained. The air spring is represented as k_a (N/m)

$$k_a = \frac{\rho_0 c^2 A_l^2}{\forall} \qquad \left(\frac{N}{m}\right)$$

Equation 3-9

Noise attenuation can be represented as a pressure ratio. An equation in terms of pressure will be more useful than an equation in terms of force. In order to obtain an expression that contains the interior pressure of the cup and the exterior pressure, all of the above terms are substituted into Equation 3-1. An equation in terms of pressure is found by dividing Equation 3-1 by the area of the leak (A_l). The leak area is used because this is the area that the external pressure acts over.

$$P_o = \frac{m}{A_l}\ddot{x} + \frac{(R_r + R_w)}{A_l}\dot{x} + \frac{\rho_0 c^2 A_l^2}{\forall A_l} x \qquad (Pa)$$

Equation 3-10

The last term in Equation 3-10 represents the inner pressure of the cup. An application of the Laplace transform to Equation 3-10 and Equation 3-7 provides the following equations:

$$P_o(s) = \frac{m}{A_l} s^2 x(s) + \frac{(R_r + R_w)}{A_l} s\, x(s) + P_i(s) \qquad (Pa)$$

Equation 3-11

$$P_i(s) = \frac{\rho_o c^2 A_l}{\forall_{cup}} x(s) \qquad (Pa)$$

Equation 3-12

This transform assumes zero initial conditions. Equation 3-12 is coupled with Equation 3-11 to yield a final transfer function that relates the inner pressure of the resonator to the ambient pressure outside the resonator.

$$\frac{P_i(s)}{P_o(s)} = \frac{\rho_o c^2 A_l^2}{\forall_{cup} m s^2 + \forall_{cup} (R_r + R_w) s + \rho_o c^2 A_l^2}$$

Equation 3-13

Equation 3-13 is the equation used to model the Helmholtz trends in the ear cup. This equation has two poles, and no zeros. A Bode plot of this transfer function will yield a 40-dB/decade roll off after resonance. While this is important information, for modeling purposes, it is desirable to know how each term is going to affect the location and magnitude of the resonance.

3.1.1 Helmholtz Model Analysis

Successful analysis of the ear cup depends on a comprehensive understanding of the fundamental physics that govern the dynamics of the ear cup. The previous section outlined the physics and equations of the Helmholtz resonator. This section examines the relative effects of the variables.

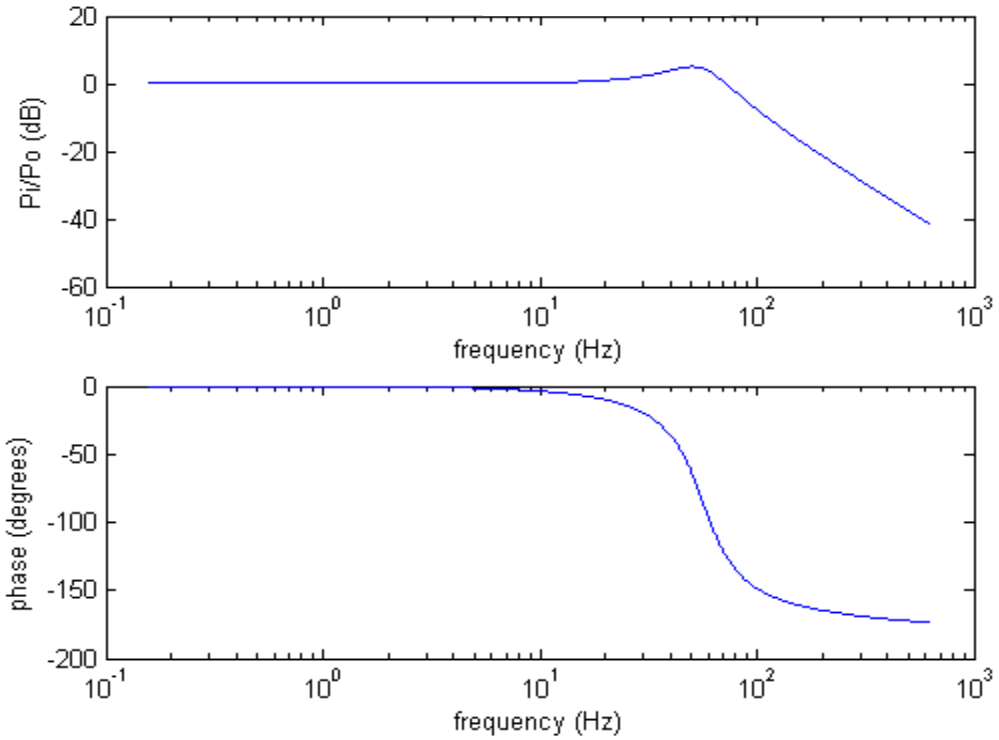

Figure 3.5: Bode plot of a Helmholtz resonator

Figure 3.5 is the Bode plot of Equation 3-13. This plot was created using realistic values that would be seen in the ear cup. The values of the key parameters used are:

ρ_o=1.29 kg/m^3	(density of air at STP)
V = .0003088 m^3	(cup volume)
L = .0127 m	(leak length)
a = .0022 m	(leak radius)
gamma = 1.4	(specific heat ratio)
Pr = .706	(Prandtl number)
η = 184e^{-7} N*s/m^2	(viscosity)
c = 343 m/s	(speed of sound at STP)

It is not of great interest to look at the effects of physical properties such as density, specific heat ratio, or the speed of sound. These parameters remain relatively constant in most any environment the ear cup is used. The variables of concern are the leak length, leak area, and cup volume. The tools used to evaluate the effect of individual variables on the Helmholtz mode will be analytical and graphical. The plots displayed in this section have darker lines to represent an increasing value of a specific parameter.

The characteristic equation of Equation 3-13 is used to analyze the results of the following plots.

$$\underset{Mass}{\left\{\forall_{cup} m\right\}} s^2 + \underset{Damping}{\left\{\forall_{cup}(R_r + R_w)\right\}} s + \underset{Stiffness}{\left\{\rho_o c^2 A_l^2\right\}} = 0$$

Equation 3-14

Equation 3-14 is the characteristic equation of Equation 3-13. It is presented in three components that dominate the dynamics of a second order system.

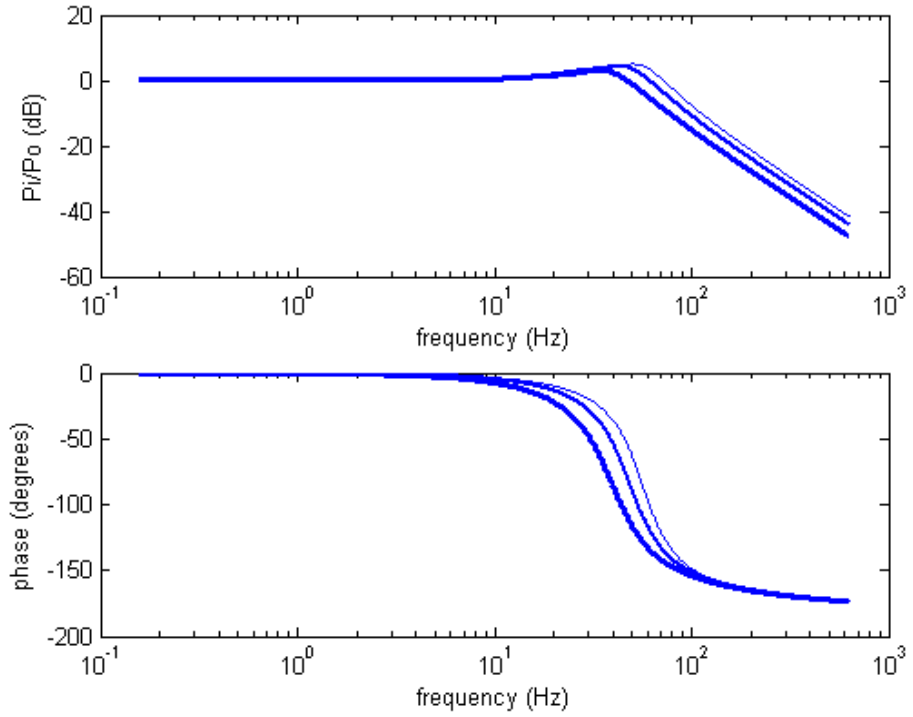

Figure 3.6: Bode plot of Helmholtz resonator with increasing cup volume

Figure 3.6 illustrates the effect that cup volume has on the dynamics of the Helmholtz mode. As stated earlier, the darker lines represent increasing values of cup volume. There are two distinct trends that can be seen with increasing cup volume. The first is a decrease in the magnitude of the resonant frequency. This parameter is governed by the damping and stiffness term of Equation 3-14. Volume is a multiplier of the damping term, but does not affect the stiffness. Since it is in the denominator of the transfer

function, as cup volume increases, the magnitude of the resonance will decrease. The second trend is a lowering of the resonant frequency. The mass and the stiffness of the system affect the frequency of resonance. The stiffness term of Equation 3-14 is not affected by the volume change of the cup, but the mass term is. The mass increases, and thus the resonant frequency decreases. In reality, the stiffness of the air spring decreases with an increase in volume as seen in Equation 3-9. The characteristic equation could be manipulated to represent the physics more accurately, but the trends it displays are still representative of the actual system.

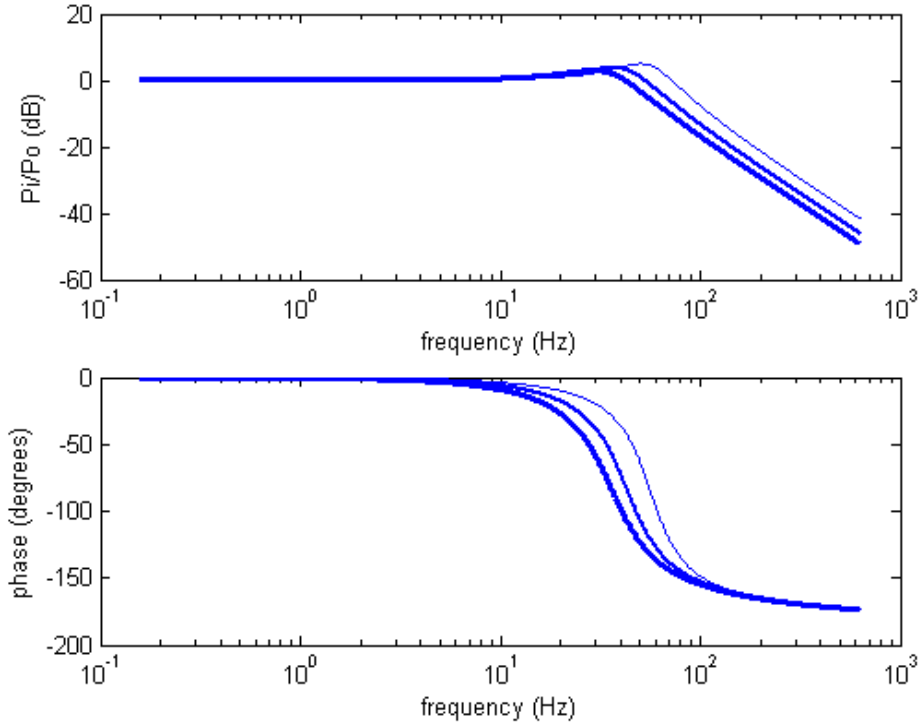

Figure 3.7: Bode plot of the Helmholtz resonator with increasing leak length

Figure 3.7 exhibits the same trend as seen Figure 3.6. The mass and the damping both increase as the leak length increases. Even though increasing the leak length is not the same as increasing the cup volume, it does produce the same trend.

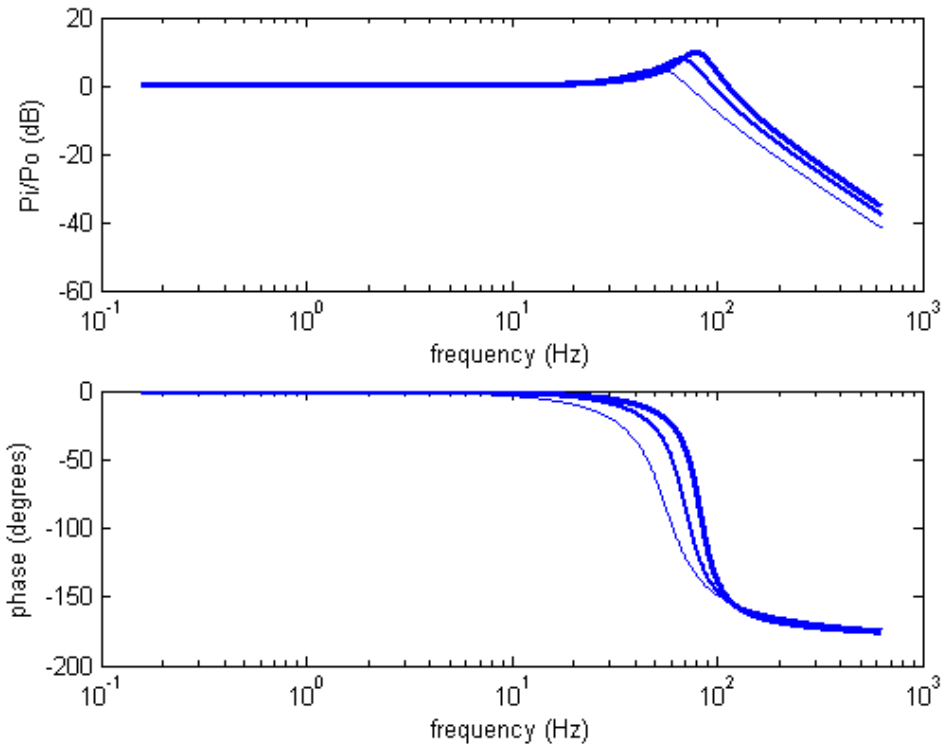

Figure 3.8: Bode plot of Helmholtz resonator with increasing leak area

Figure 3.8 shows how an increase of leak area impacts the Helmholtz dynamics. Referring to Equation 3-14, all the terms are a function of leak area, but the end result is an increase in the stiffness term. Every term in the characteristic equation is increasing linearly as a function of leak area with the exception of the stiffness and the radiation resistance. These two terms increase with the square of leak area. Since the stiffness of the system is increasing more rapidly than the mass, it is consistent that the location of resonance increases with leak area. What is not clear is why the damping does not stay the same as leak area increases.

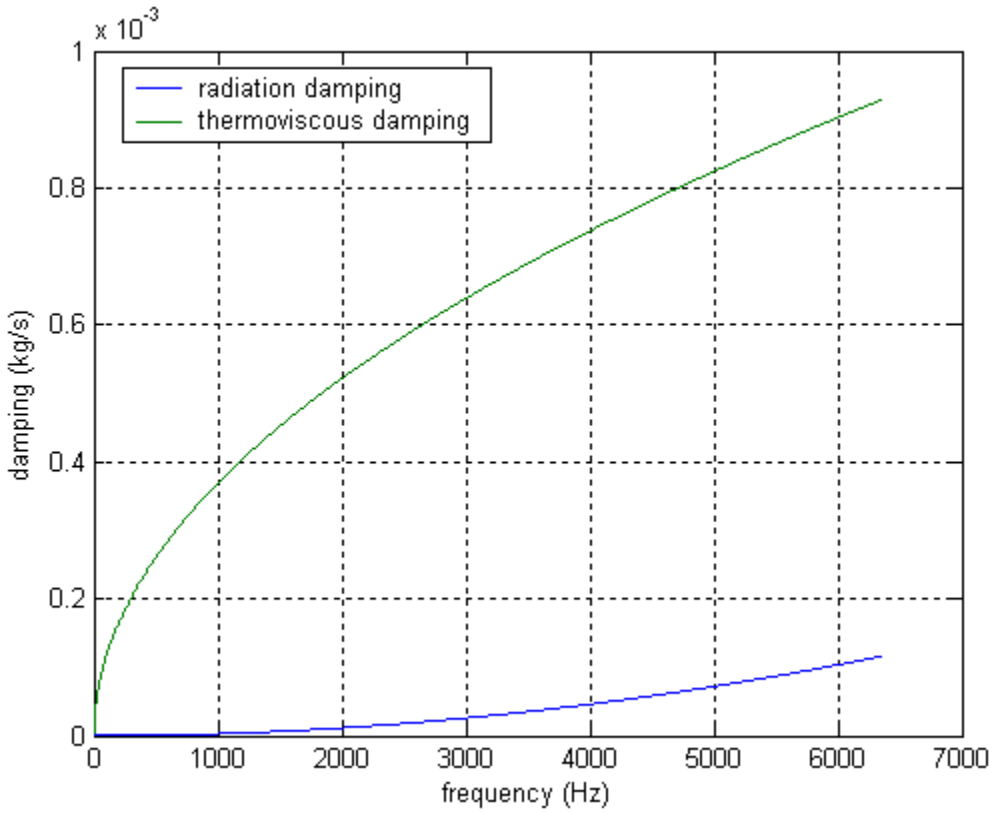

Figure 3.9: Comparison of resistance terms

Figure 3.9 shows that below 1000 Hz, the radiation resistance is many orders of magnitude lower than the thermoviscous damping. This means that the damping is not increasing proportionally to the stiffness, and thus the magnitude of the resonance increases with an increase of leak area.

In a normal ear cup, the variable that will change the most from person to person is the leak area. This is due primarily to the varying shapes of the skull around the ear. It is also possible to create more than one leak around the ear. This analysis is limited to a single leak. The previous analysis does not provide any more information than a trend. Because the leak area is a widely varying parameter, a more detailed analysis is required.

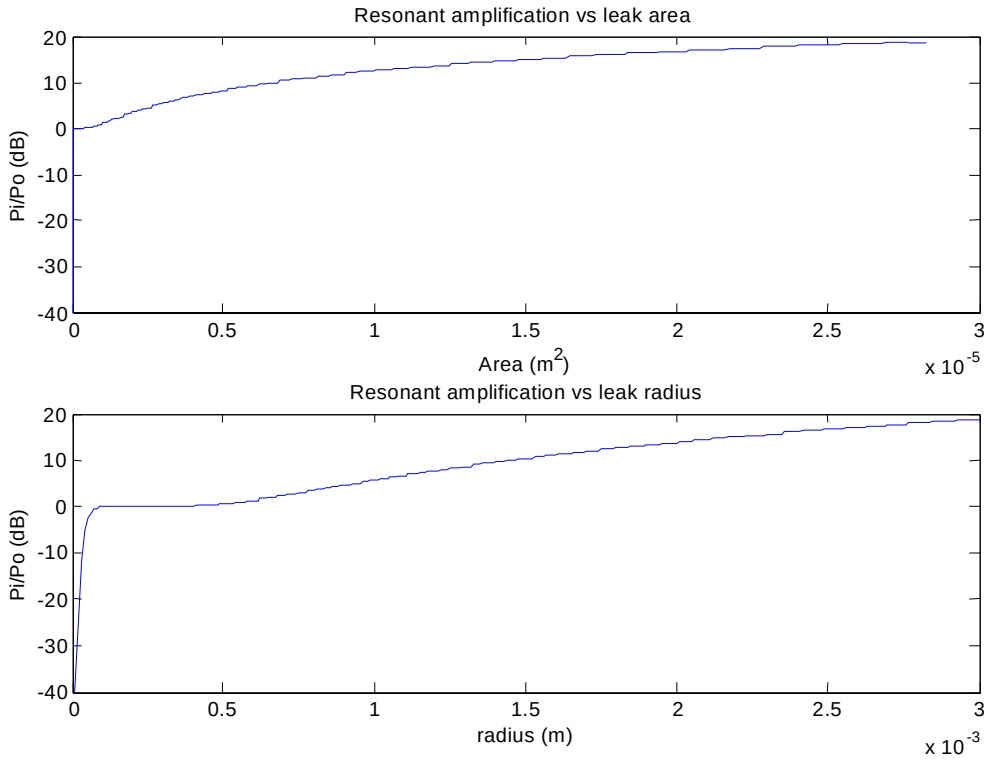

Figure 3.10: Resonant amplification of Helmholtz resonator as leak area increases

Figure 3.10 shows how the magnitude of resonance varies as the leak size increases. For small leak sizes (.2 mm - .4 mm radius) there is no amplification of noise within the cup. This is due primarily to very low corresponding resonant frequency and high viscous losses. As the leak area increases, and the stiffness becomes more dominant than the damping, the resonant magnitude increases.

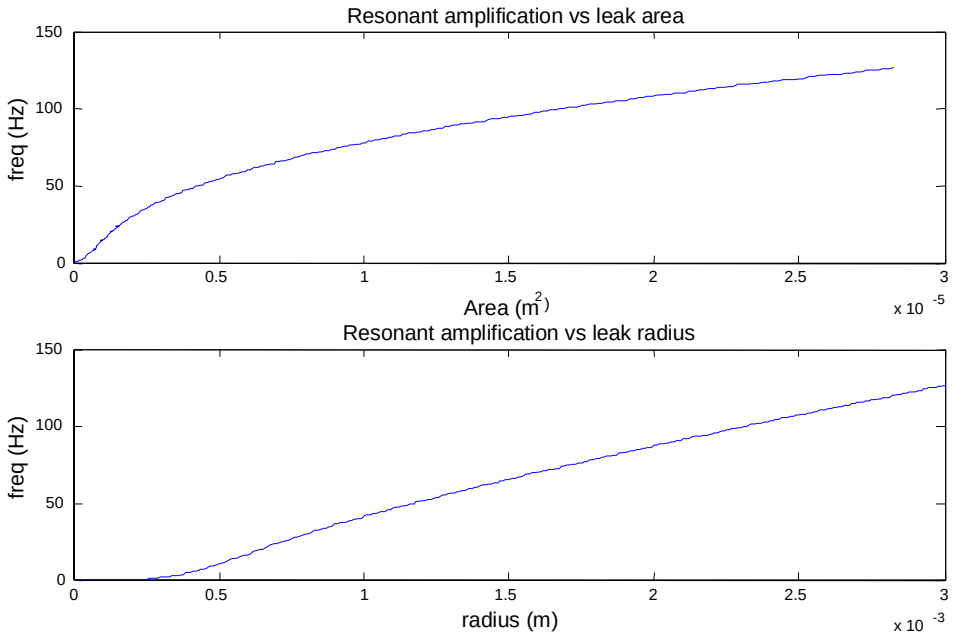

Figure 3.11: Resonant frequency of Helmholtz as leak area increases

Figure 3.11 shows the location of the resonant frequency as a function of leak area. Comparing Figure 3.11 to Figure 3.10, it can be noted that the resonant frequency is very nearly 0 Hz until pressure amplification begins to occur. This implies that there is no energy entering the system. Just as the slope of the pressure changes at .4 mm, so does the slope of the resonant frequency.

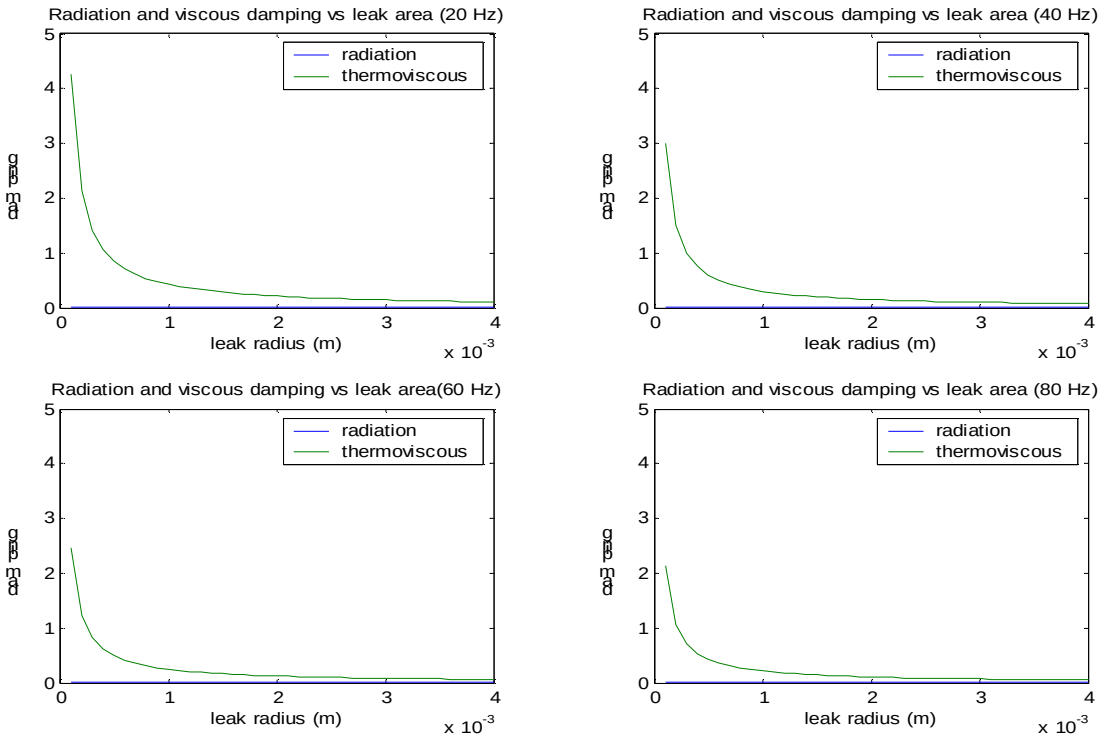

Figure 3.12: Radiation and viscous damping as leak area increases for different resonant frequencies

Figure 3.12 shows that the radiation damping is negligible compared to the viscous damping. The viscous damping decreases as the frequency increases and as the leak area increases. This correlates well with Figure 3.10 and Figure 3.11. Less energy is absorbed through viscous damping at higher frequencies; therefore the remaining energy is put into the system. This causes the increased pressure amplitudes seen as the leak area is increased.

3.1.2 DC Gain of the Helmholtz Resonator

The previous analysis focused on the dynamic response of the Helmholtz resonator. This section looks at the steady state, non-dynamic characteristics of the ear cup. The DC gain is seen throughout the frequency band of a system. Understanding the parameters that affect the DC gain is necessary for effective cup design. The DC gain of the Helmholtz resonance can be found by revisiting Equation 3-13.

$$\frac{P_i(s)}{P_o(s)} = \frac{\rho_o c^2 A_l^2}{\forall_{cup} m s^2 + \forall_{cup}(R_r + R_w)s + \rho_o c^2 A_l^2}$$

Currently Equation 3-13 is represented in the Laplace domain. Converting Equation 3-13 into the frequency domain and letting the frequency approach zero will provide Equation 3-15.

$$\frac{P_i(j\omega)}{P_o(j\omega)} = \frac{\rho_o c^2 A_l^2}{\rho_o c^2 A_l^2} = 1$$

Equation 3-15

Equation 3-15 clearly shows that there can be no DC gain in the Helmholtz resonance. As the frequency approaches zero, the pressure will equalize in the cup volume. This suggests that there is no design that can be implemented that will affect the static response of the Helmholtz mode. This will not be the case with the piston resonance.

3.1.3 Effects

The Helmholtz resonator equations are derived with the assumption that the fluid in the leak moves as a piston. This was assumed to be true up through 2700 Hz, but at higher frequencies, this assumption may not be valid. Previous studies have suggested that the leak does not contribute any energy to the system at higher frequencies. This assertion may not be the case. A look at a transfer function between acceleration and force may lead to different conclusions.

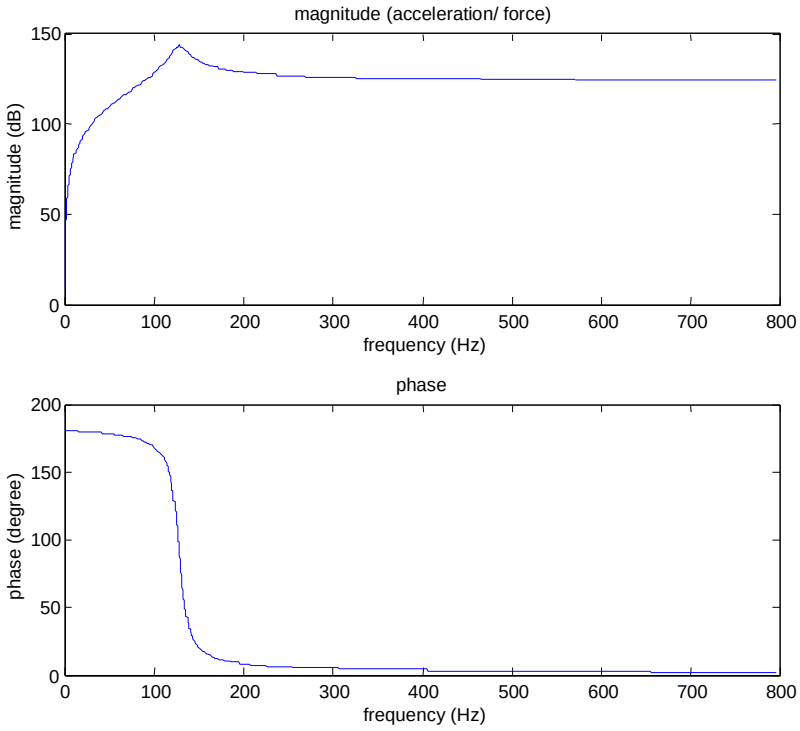

Figure 3.13: Bode plot of acceleration/ force

Figure 3.13 is the Bode plot of acceleration and force for the Helmholtz resonator. After resonance, the acceleration of the fluid remains constant as a function of frequency. Acceleration of the fluid requires that a force act on it. The force is exerted on the fluid by the internal and external pressure acting over the area of the leak. This means that the cup will have to maintain a nominal pressure as frequency increases in order to maintain a constant acceleration of the fluid. Once the fluid becomes compressible, new assumptions must be made to characterize the leak.

3.2 Piston Resonance

Regardless of sealing, or user fit, a mechanical resonance exists in circumaural ear protectors. This resonance transmits sound directly to the ear. The mechanical resonance of the ear cup has been the focus of previous ear defender research, and has been well documented (Shaw, 1958). Shaw found that increasing three parameters; the seal stiffness, the cup volume, and the band force on the head could minimize vibration, and thus minimizes sound transmission to the ear.

The mechanical resonance of the DCCI 9AN/2 ear cup is modeled as a spring-mass-damper system. The ear cup and the seal material represent the mass of the system. In this model, however, the mass of the seal is neglected. The damping of the system is represented entirely by the seal. In practice, the seal has stiffness and damping characteristics. This is known as a complex stiffness. In this model, it is more convenient to separate the complex stiffness into its real terms, damping and stiffness. The seal and the air spring represent the entire stiffness of the system.

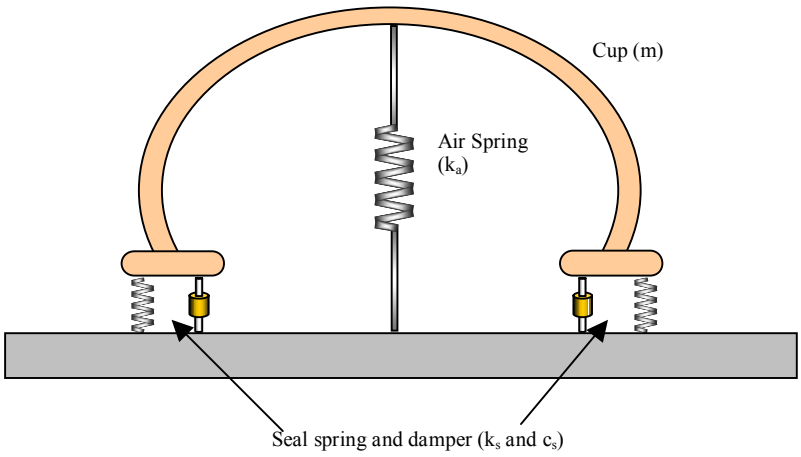

Figure 3.14: Spring-mass-damper system of the no leak case

Figure 3.14 is a representation of the system that is modeled in this section. In this model, the seal spring and the air spring act in parallel. This results in an addition of the spring terms. As mentioned earlier, the mass of the seal is neglected in this model. The

vibration of this system is assumed to be on a single axis. Only the forces that act on the axis of motion will be considered in the derivations.

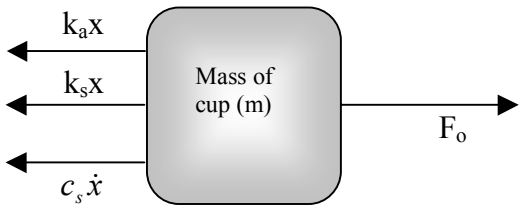

Figure 3.15: Free body diagram of no leak case

The free body diagram seen in Figure 3.15 represents the forces acting on the cup. The forces on the left side of the diagram represent the air spring, seal spring and the damper. The force acting on the cup (F_o) is a function of the ambient pressure.

$$m\ddot{x} + c_s\dot{x} + k_s x + k_a x = F_o \qquad (N)$$

Equation 3-16

Applying the equation of motion to the free body diagram yields Equation 3-16.

$m = m_{cup}$ (kg)
$c_s = c_{seal}$ (kg/s)
k_s = stiffness of seal (N/m)
k_a = stiffness of air (N/m)

Nearly all of the variables in Equation 3-16 can be represented as a constant. The air spring is an exception to this. As mentioned earlier, the mechanical resonance exists regardless of whether or not there is a leak in the cup. Modeling the air spring is greatly simplified if it assumed that there is no leak in the cup. The assumption of a leak leads to a coupled air-spring term. This coupled analysis will be covered in section 3.3.

$$k_a = \frac{\rho_o c^2 A_i A_s}{\forall_{cup}}$$

Equation 3-17

The expression for the air spring in Equation 3-17 is derived using the ideal gas law. The derivation is the same method used for the air spring in the Helmholtz resonator.

A_i = projected area that internal pressure acts on
A_s = area that the seal compresses around
c = speed of sound at STP
ρ_o = density of air at STP

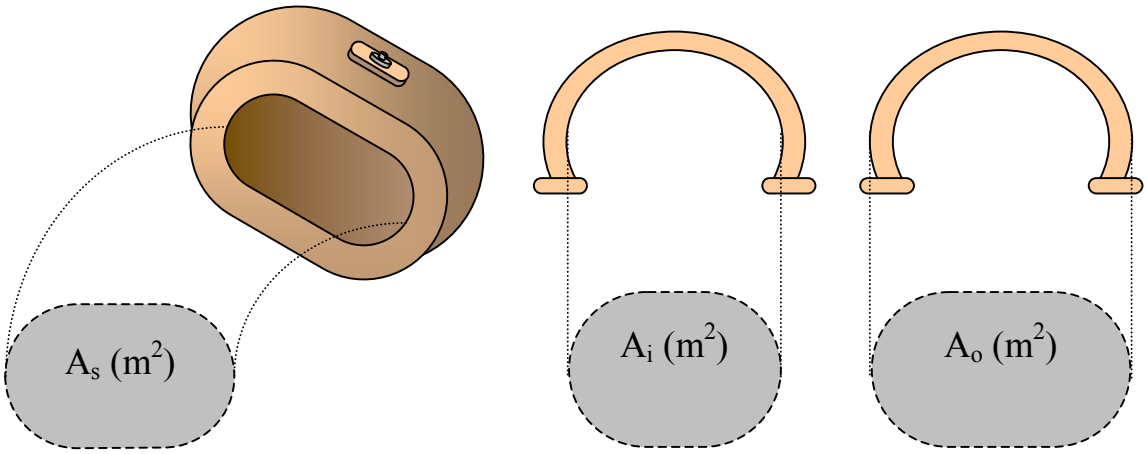

Figure 3.16: Area terms for spring stiffness term

The area, A_s, seen in Figure 3.16 also corresponds to the open area of the seal. A_i is the projected area of the interior of the ear cup. Both areas are perpendicular to the axis of vibration.

The goal of this analysis is to create a transfer function that compares the interior pressure of the ear cup, to an external excitation pressure. The next step towards achieving this goal is to transform Equation 3-16 into a function of pressure. Pressure is simply force divided by the area it acts on. The excitation pressure acts over the external projected area of the cup.

$$m\ddot{x} + c_s\dot{x} + k_s x + k_a x = A_o P_o$$

Equation 3-18

Equation 3-18 is the equation of motion transformed into a function of external pressure. This equation does not yet have an internal pressure term, which is required to form a transfer function between the internal and external pressure. The air spring will provide

the necessary equation to introduce the internal pressure to the modified equation of motion. Similar to any other spring, the force required to compress the air spring is related by Hooke's law. The force exerted by the air spring acts over the projected area of the inner cup.

$$P_i = \frac{k_a x}{A_i} \qquad (Pa)$$

Equation 3-19

Equation 3-18 contains the numerator of Equation 3-19. Dividing Equation 3-18 by the projected internal area of the ear cup yields an expression that includes the internal pressure of the ear cup.

$$\frac{m\ddot{x} + c_s\dot{x} + k_s x}{A_i} + \frac{k_a x}{A_i} = \frac{A_o}{A_i} P_o$$

Equation 3-20

Equation 3-20 is now in a form in which the internal pressure of the ear cup can be introduced. Adding the internal pressure term and taking the Laplace transform leads to the final transfer function between the internal pressure of the ear cup and the excitation pressure.

$$\frac{P_i(s)}{P_o(s)} = \frac{A_o}{A_i}\left(\frac{k_a}{ms^2 + c_s s + (k_s + k_a)}\right)$$

Equation 3-21

Equation 3-21 is plotted below, using realistic values for the ear cup.

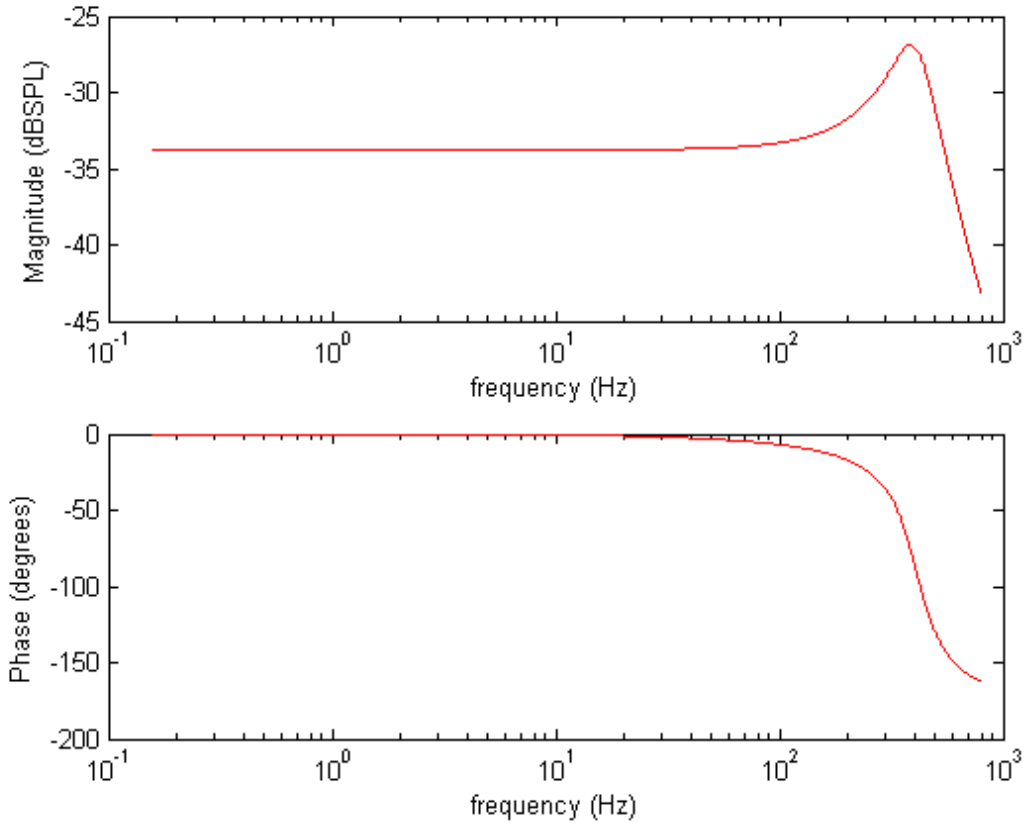

Figure 3.17: Bode plot of pressure ratio for no leak head cup

The values of the key parameters used are:

ρ_o=1.29 kg/m^3
V = .0003088 m^3
c = 343 m/s
A_i = .0025 m^2
A_o = .003 m^2
m_{cup} = .02 kg
k_s = 130000 kg/s^2
c_s = 20 kg/s

Figure 3.17 represents the Bode plot of the no leak condition. Just like other spring-mass-damper systems, the magnitude decays as frequency extends into the mass controlled region. Unlike the Helmholtz resonator, the mechanical resonance does not have a trivial solution for the DC gain.

3.2.1 DC Gain of the Piston Resonance

The importance of the DC gain was mentioned in the Helmholtz section. The DC gain term adds a bias to the response of the system. The DC gain of the mechanical resonance is obtained in the same manner as the Helmholtz resonance. Transforming Equation 3-21 into the frequency domain yields the following expression.

$$\frac{P_i(j\omega)}{P_o(j\omega)} = \frac{A_o}{A_i}\left(\frac{k_a}{m(j\omega)^2 + c_s(j\omega) + (k_s + k_a)}\right)$$

Equation 3-22

The DC gain is the term left over after all the frequency dependant terms have been set to 0. The result of setting ω to 0 in Equation 3-22 can be seen below.

$$\frac{P_i(s)}{P_o(s)} = \frac{A_o}{A_i}\left(\frac{k_a}{(k_s + k_a)}\right)$$

Equation 3-23

Equation 3-23 is a function of cup geometry and spring rates. The air spring, k_a, is also a function of the cup geometry. A more useful expression is obtained by substituting the expression for the air spring into Equation 3-23.

$$\frac{P_i(s)}{P_o(s)} = \frac{A_o}{A_i}\left(\frac{\rho_o c^2 A_i A_s}{k_s \forall + \rho_o c^2 A_i A_s}\right)$$

Equation 3-24

It was mentioned at the beginning of section 3.2 that Shaw had identified three parameters that would influence attenuation to the ear; cup volume, seal stiffness, and headband force (Shaw, 1958). The seal stiffness and cup volume are identified in Equation 3-24 as key parameters that influence the DC gain of the mechanical resonance. The band force is not accounted for in this expression. The cup geometry has little influence on the DC gain of the system, with the exception of the interior and exterior projected areas. In the DCCI 9AN/2 cup, the area terms are very similar, and thus A_o/A_i will approach unity. Doubling the cup volume would render the ear cup impractical. Realistically, the only parameter than can impact the DC gain of the mechanical

resonance is the seal stiffness. The seal stiffness term can be adjusted by many orders of magnitude. The only constraint on this parameter is the comfort of the user.

3.3 Coupled Response of Helmholtz and Piston Resonance

Two individual phenomena that affect the noise attenuation within the ear cup have been identified; the Helmholtz resonance, and the piston resonance. These two dynamics rarely occur exclusively of one another in an ear cup. Each resonance is coupled to the other through the fluid medium, and therefore must truly be considered using dynamic models of the coupled system. This requires that there be a coupled analysis of these two resonances.

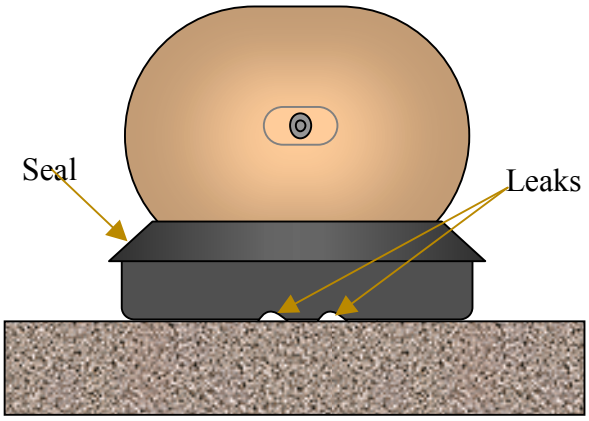

Figure 3.18: Cup with seal and leak

Figure 3.18 is an illustration of the DCCI ear cup with a DCCI undercut foam seal. With leaks introduced at the base of the seal, the ear cup in Figure 3.18 meets the requirements for the piston and Helmholtz resonator.

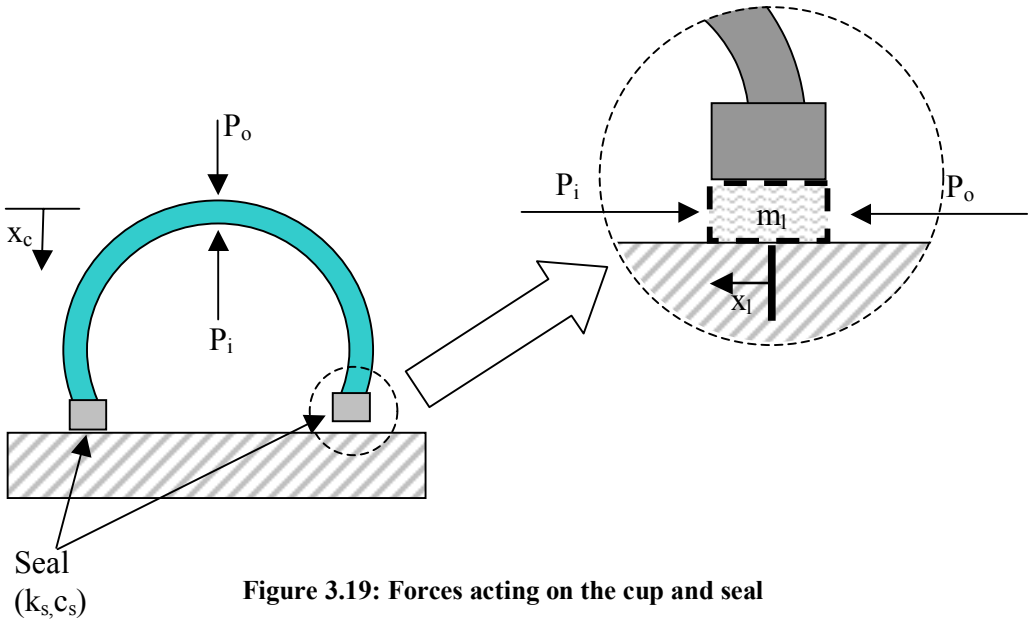

Figure 3.19: Forces acting on the cup and seal

Figure 3.19 is an illustration of the coupled system shown with forces. The system is coupled through the internal volume of the cup. Movement in either coordinate system affects the internal volume of the cup. Using the ideal gas assumption and the coupled coordinate system, an expression for the internal pressure of the cup can be found (Homma 2004).

$$P_i = \frac{\rho c^2 A_s}{\forall_{cup}} x_c + \frac{\rho c^2 A_l}{\forall_{cup}} x_l$$

Equation 3-25

where

A_s = effective cup surface area (m^2)
A_l = leak opening area (m^2)
x_l = leak displacement coordinate (m)
x_c = cup displacement coordinate (m)

The variables used in Equation 3-25 are the same variables used in the Helmholtz and Piston resonance analyses. The solution of the coupled system response is simplified by transforming the internal pressure equation into vector form. Equation 3-25 is represented in vector form below (Homma 2004).

$$P_i = \frac{\rho c^2}{\forall_{cup}} \cdot \vec{a}^T \cdot \vec{x}$$

Equation 3-26

where

$$\vec{a} = \begin{bmatrix} A_s \\ A_l \end{bmatrix}, \qquad \vec{x} = \begin{bmatrix} x_c \\ x_l \end{bmatrix}$$

An expression for the external pressure of the system is found through Hooke's law. The external pressure exerts a force on the cup that can be quantified by the displacement of the system. This displacement is a function of the stiffness of the system (Homma 2004).

$$\vec{k} \cdot \vec{x} = \vec{a} \cdot P_o$$

Equation 3-27

Where

$$\bar{k} = \begin{bmatrix} m_c s^2 + c_s s + (k_s + ka_c) & \frac{\rho c^2 A_l A_s}{\forall} \\ \frac{\rho c^2 A_l A_s}{\forall} & m_l s^2 + c_l s + ka_l \end{bmatrix}$$

$s = j\omega$
c_s = seal damping coefficient
c_l = damping coefficient for leakage
k_s = seal stiffness
ka_c = air spring stiffness as seen by the cup
ka_l = air spring stiffness as seen by the leak

The expressions for the air stiffness are defined as:

$$ka_c = \frac{\rho c^2 A_s^2}{\forall} \qquad \left(N/m\right)$$

$$ka_l = \frac{\rho c^2 A_l^2}{\forall} \qquad \left(N/m\right)$$

$$P_i = \frac{\rho c^2}{\forall_{cup}} \cdot \vec{a}^T \cdot \vec{x}$$

Equation 3-26 and Equation 3-27 can be combined to create a transfer function between the interior and exterior pressure of the cup (Homma 2004).

$$\frac{P_i}{P_o} = \frac{\rho c^2}{\forall_{cup}} \vec{a}^T \bar{k}^{-1} \vec{a}$$

Equation 3-28

The result of Equation 3-28 using realistic parameters can be seen below.

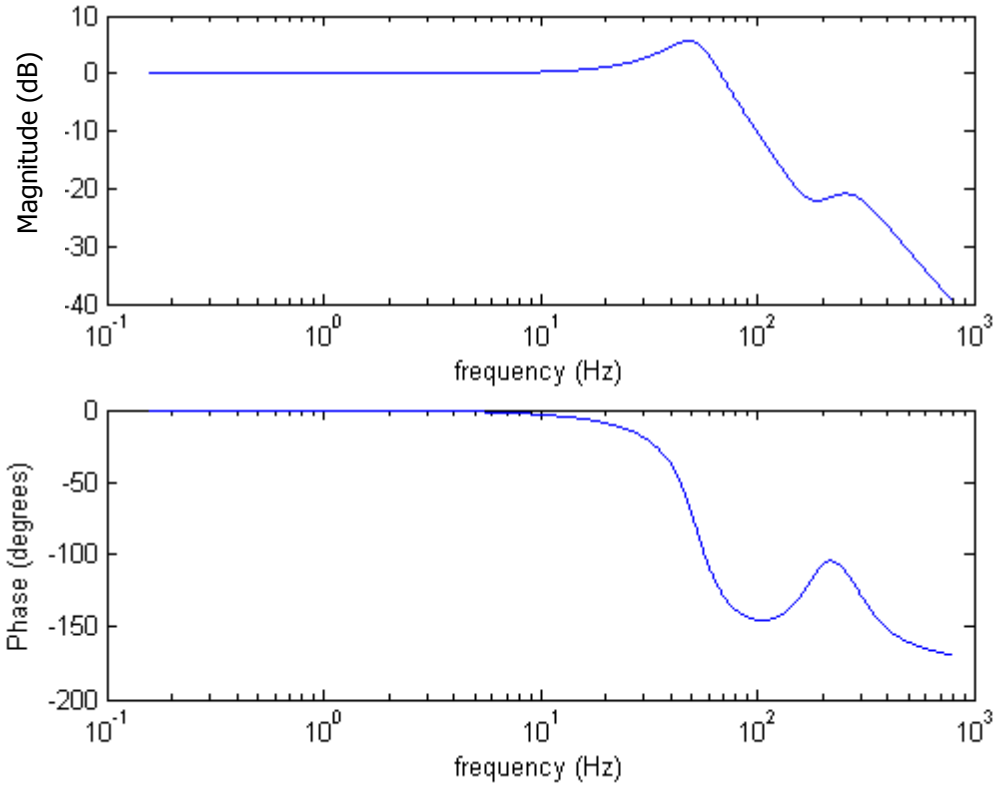

Figure 3.20: Two degree of freedom model

Figure 3.20 displays the results of the coupled system. The first resonance represents the contribution of the Helmholtz resonator. This resonance exhibits the same characteristics exposed in the Helmholtz section. The DC gain of the system is 0 dB, and the resonance occurs at a low frequency. The Helmholtz resonance dominates the coupled system until 100 Hz. At this point, the phase begins to increase. At about 190 Hz the piston resonance dominates the magnitude of the coupled system. If the leak size

is increased, it is possible for the Helmholtz resonance to completely mask the effects of the piston resonance.

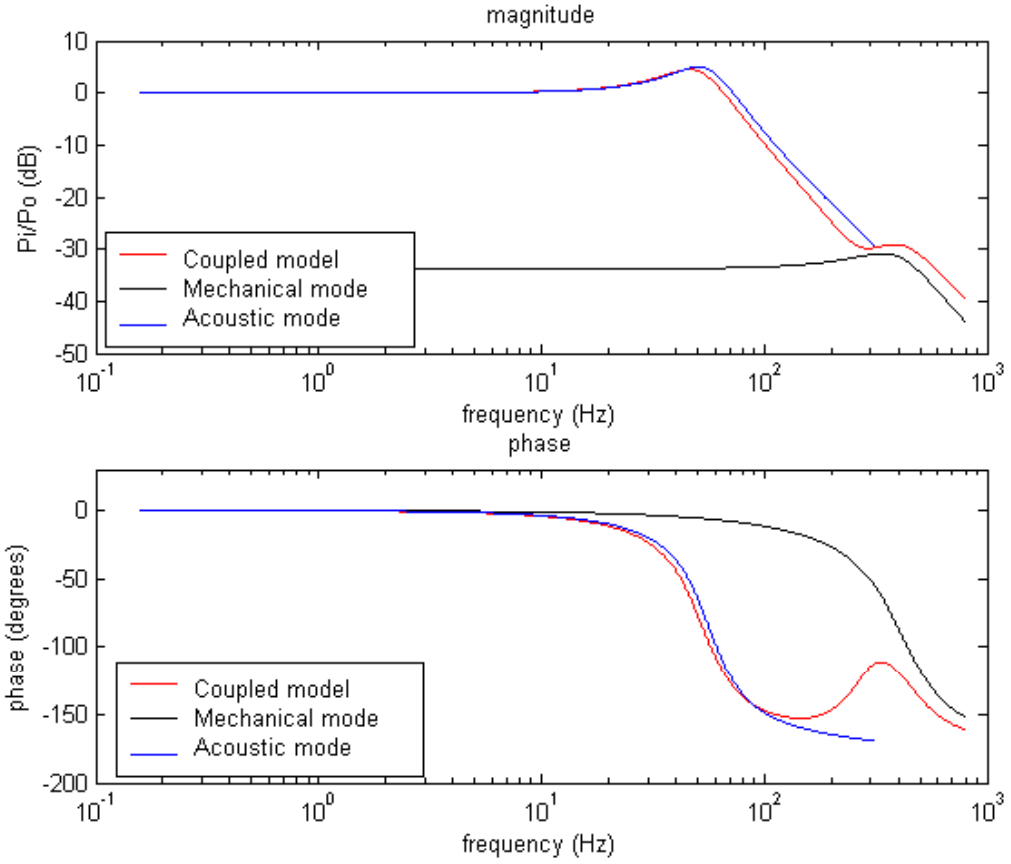

Figure 3.21: Comparison of piston mode Helmholtz mode and 2DOF

Figure 3.21 is a comparison of the piston resonance, Helmholtz resonance, and the coupled response of the two phenomena. The coupled model predicts the individual resonances well. The coupled model shows attenuation between the two resonances. This suggests that the piston resonance destructively interferes with the Helmholtz resonance in this region. The coupled response shows lower attenuation than the piston resonance alone. This then implies that the Helmholtz resonance is constructively interfering with the mechanical resonance. This idea will be explored more closely when the velocity of the leak is analyzed.

3.4 Leak Velocity of the Helmholtz Resonator

The analysis of the coupled response of the Helmholtz and piston resonances exposed decay in attenuation after the piston resonance. One way to explain this decay in attenuation is to explore the acceleration of fluid within the leak. A leak in the ear cup can be viewed as a source term that can add energy into the system across a large frequency range. In this case, energy is added to the system by air accelerating back and forth within the leak. Experimentally, the most convenient way to measure the acceleration of fluid in the leak is by measuring its velocity.

For this type of testing, we will not be measuring an average velocity. The average velocity of the fluid in the leak will nearly be zero, and no information can be gained from this. Instead, the unsteady velocity of the fluid will provide the necessary information to find the acceleration of the fluid in the leak area. The most effective way to find the unsteady velocity is to use two pressure sensors in the leak area, and relate their pressure to velocity using Euler's equation.

$$-\frac{\partial p}{\partial x} = \rho \frac{\partial u'}{\partial t}$$

Equation 3-29

A known distance separates the microphones, and the density of air is known. With some manipulation, the acoustic velocity is found to be:

$$u' = \frac{1}{\rho \Delta x} \int p_1 - p_2 \, dt$$

Equation 3-30

Experimentally evaluating Equation 3-30 can be done a number of different ways. The simplest way to evaluate the expression would be to take the pressure data, and have a computer solve for the unsteady velocity. Another option is to build an analog circuit that will solve for the unsteady velocity. Because it is desirable to have a transfer function with respect to velocity, it will be necessary to build an analog circuit. This

necessity arises due to input limitations of the data acquisition machine used for this testing.

3.4.1 Leak Velocity Modeling

This section focuses on modeling the velocity of the slug of fluid within the leak of the Helmholtz resonator. It is of interest to know how the leak velocity is affected by external pressure. It is also of interest to understand how the leak velocity affects the internal pressure. The first transfer function is easily found using Equation 3-1 transformed into the s domain.

$$F_o(s) = ms^2 x(s) + c_a s\, x(s) + k_a\, x(s)$$

Equation 3-31

The velocity term, s x(s) can be pulled out of Equation 3-31 to yield a transfer function between the external pressure and velocity.

$$\frac{V(s)}{F_o(s)} = \frac{1}{ms + c_a + \frac{k_a}{s}}$$

Equation 3-32

Equation 3-32 is a generic transfer function that can be applied to any second order system. It is now only necessary to transform the force to a pressure. The outside pressure is related to the force by the leak area. Changing the force to outside pressure provides the final form of the transfer function.

$$\frac{V(s)}{P_o(s)} = \frac{A_l s}{ms^2 + (R_r + R_w)s + k_a}$$

Equation 3-33

where

m = mass of fluid in the leak (kg)
A_l = area of the leak opening (m^2)
k_a = stiffness of the air spring (N/m)

R_r = radiation resistance (kg/s)
R_w = thermoviscous resistance (kg/s)

Equation 3-33 is very similar to the transfer function for the Helmholtz resonator. The primary difference between the two is a zero at the origin. This changes the initial phase angle, and the magnitude information. Equation 3-33 is plotted below using realistic values for the Helmholtz resonator.

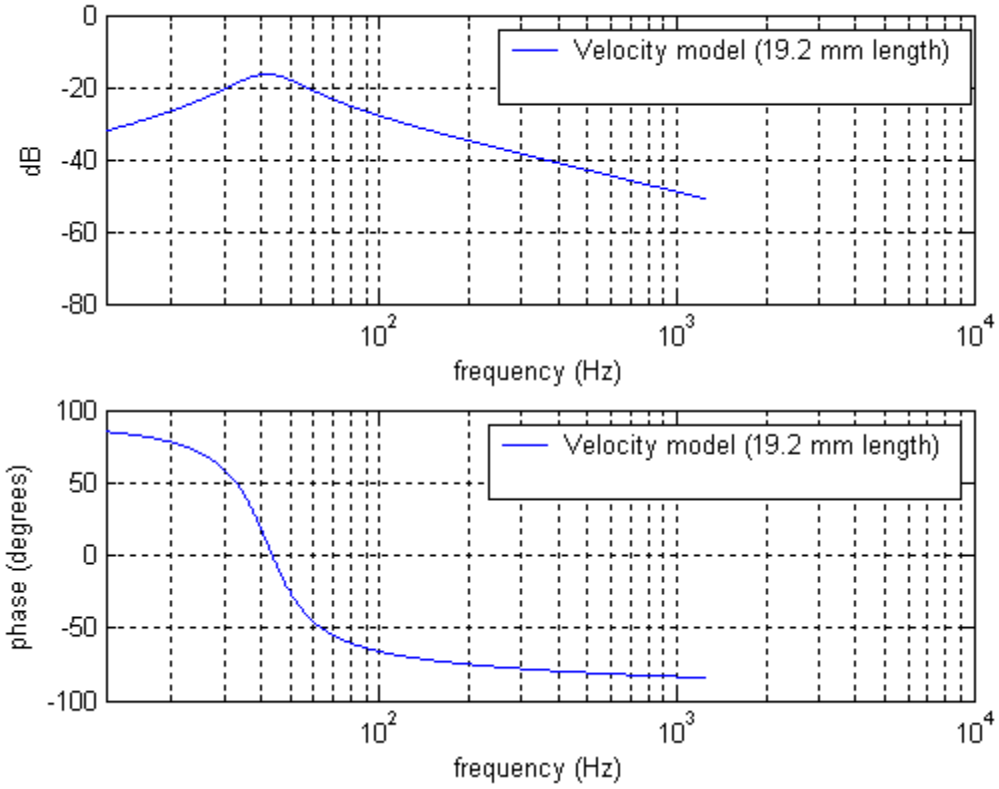

Figure 3.22: Plot of leak velocity as a function of external pressure (Al = 67.2e-7)

Figure 3.22 is a plot of the leak velocity as a function of the external pressure. This figure corresponds to a constant acceleration of the fluid. Figure 3.22 will be compared to experimental data to determine the frequency range that the leak adds energy to the system. The next step is to find out how the leak velocity affects the internal pressure of the cup. Finding this expression requires Equation 3-13 and Equation 3-33. Equation 3-13 can be re-written in terms of outside pressure.

$$P_o(s) = P_i(s)\frac{\forall_{cup} ms^2 + \forall_{cup}(R_r + R_w)s + \rho_o c^2 A_l^2}{\rho_o c^2 A_l^2}$$

Equation 3-34

$$P_o(s) = P_i(s)\frac{\forall_{cup} ms^2 + \forall_{cup}(R_r + R_w)s + \rho_o c^2 A_l^2}{\rho_o c^2 A_l^2}$$

Equation 3-34 is then substituted into Equation 3-33.

$$\frac{V(s)}{P_i(s)\dfrac{\forall_{cup} ms^2 + \forall_{cup}(R_r + R_w)s + \rho_o c^2 A_l^2}{\rho_o c^2 A_l^2}} = \frac{A_l s}{ms^2 + (R_r + R_w)s + k_a}$$

Equation 3-35

Equation 3-35 can be simplified to provide the final form of the equation to be used.

$$\frac{P_i}{V} = \frac{\rho_o c^2 A_l}{\forall_{cup} s}$$

Equation 3-36

Equation 3-36 contains a single pole at the origin. This will provide a plot that has a slope of –20 dB/decade, and a constant phase of –90 degrees.

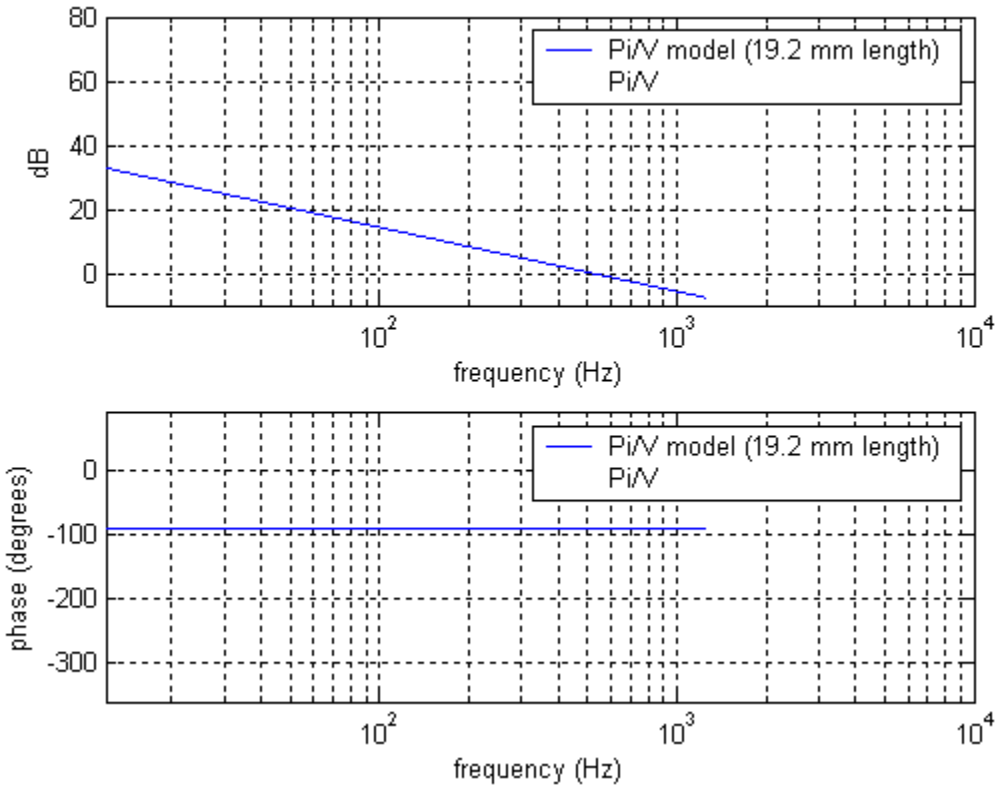

Figure 3.23: Plot of internal pressure as a function of leak velocity

These two plots will be used to see how well the experimental data matches with the models.

4 Testing

Experimental validation of analytical models is the natural progression of research. In Chapter 3, a number of models were derived to explain the low frequency dynamics that occur within the ear cup. The work outlined in this chapter sets out to validate these models with physical experiments. In addition to this work, experiments were also conducted to explore the effects of a foam insert and the effect of mid-frequency mode shapes within the ear cup.

4.1 Helmholtz Resonator Testing

Until now, the Helmholtz resonance has not been documented as a contributing dynamic to noise attenuation loss in ear cups. The primary goal of this set of tests was to prove that the Helmholtz resonance exists within ear cups. The secondary goal was to show that the derived Helmholtz models fit the data well. The test results show that the Helmholtz resonance does exist within the ear cup, but the data does not match the model accurately. This discrepancy will be discussed later.

4.1.1 Experimental Set Up

In order to isolate the Helmholtz resonance in the ear cup, it was necessary to design an experiment that met the assumptions of the model as closely as possible. This meant using a seal that was nearly completely rigid, as well as securing the ear cup to a solid base. In doing this, the ear cup was turned into a rigid walled volume with a leak. A section was taken out of the seal material in order to create the leak.

Figure 4.1: Stiff seal with 3/4" cutout

The seal material seen in Figure 4.1 is made from an automotive gasket material. The leak length was cut so that it was the same length as the lip of the ear cup. The next step was to secure the ear cup to a flat, rigid surface. An existing test rig was used to hold the ear cup to a plate of Plexiglas attached to particleboard.

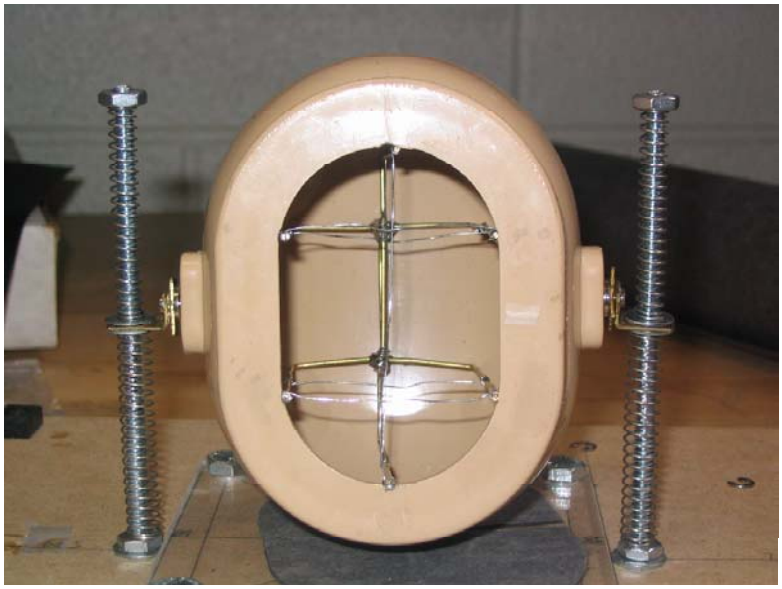

Figure 4.2: Ear cup mounting shown with microphone cage

The ear cup in Figure 4.2 is mounted in a manner that allows the user to vary the load on the ear cup. For the Helmholtz tests, the load was set to the maximum level to insure a

rigid seal. The microphone cage is also shown in Figure 4.2. This cage was designed to allow microphones to be placed in varying locations within the ear cup. For this set of tests, the microphone location within the cup is not critical because the Helmholtz resonance is a bulk effect. This means that the pressure within the cup should be uniform as long as the criteria for the Helmholtz resonator are satisfied.

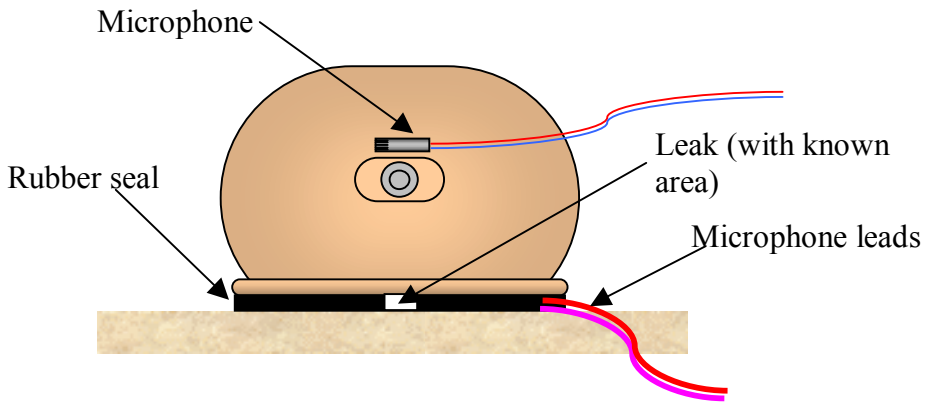

Figure 4.3: Diagram of Helmholtz testing configuration

The transfer function derived in Section 3.1.1 relates the interior pressure of the ear cup to the exterior excitation pressure. In order to find this transfer function experimentally, a microphone must be placed inside the ear cup, and one placed outside the ear cup. An illustration of this set up is seen in Figure 4.3. As mentioned earlier, the location of the interior microphone is not critical; however, the location of the exterior microphone is important. The Helmholtz resonance is excited through the leak, so it is necessary to know the pressure at the leak in order to obtain a meaningful transfer function. This is accomplished by placing an exterior microphone just outside the leak.

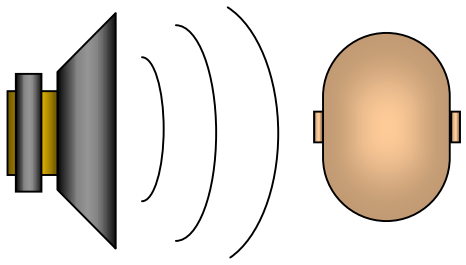

Figure 4.4: Orientation of speaker with respect to head cup

The location of the speaker affects the response of the ear cup. It was decided that the most efficient way to excite the Helmholtz resonance was to aim the speaker directly at the leak. This set up is seen in Figure 4.4.

Figure 4.5: Set up of Helmholtz tests

For all of the Helmholtz tests, the ear cup was excited with an 800 Hz random noise signal generated by an FFT analyzer. Each microphone signal was sent through a pre-amplifier to remove any DC bias between the two microphones. The two signals were then fed into the FFT to be processed. Figure 4.5 shows the final test set up of the Helmholtz tests.

4.1.2 Test Results

The Helmholtz resonance is present within the ear cup. The resonance was tested with varying leak sizes, and different microphone positions. All of the relevant parameters can be identified using the serial number for the data. A description of the serial number can be found in Appendix A.

Table 4-1: Table of leak sizes

Leak width (inches)	Leak width (m)	Leak Height (m)	Leak area (m^2)
1/8	3.02E-03	8.38E-04	2.53E-06
3/16	5.31E-03	8.38E-04	4.45E-06
3/8	9.88E-03	8.38E-04	8.28E-06
1/2	1.32E-02	8.38E-04	1.10E-05
3/4	1.86E-02	8.38E-04	1.56E-05
1	2.50E-02	8.38E-04	2.09E-05

Table 4-1 shows the leak sizes that were used for Helmholtz testing. These leak sizes are also nearly the same size leak one would expect to see when using the hearing defender.

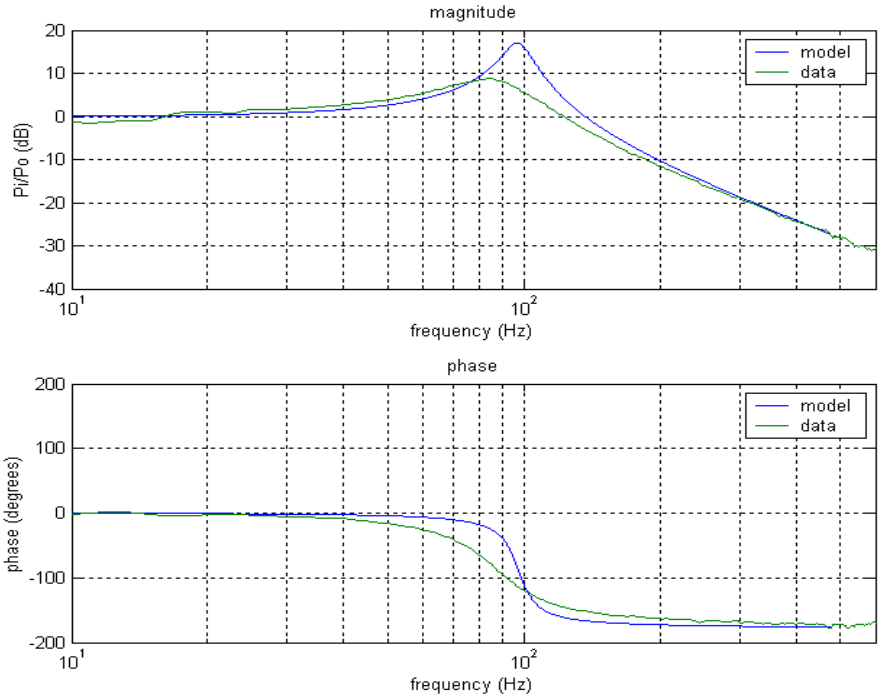

Figure 4.6: Frequency response plot of ¾" leak compared to model

The first set of data plotted is shown in Figure 4.6 (HAL-1M2-F-156). The experimental data, shown in red, nearly matches the model, but is more heavily damped. The damped natural frequencies are also different for the two plots. It appears that the model matches

the data well, but it is desirable for the model to match the experimental data more accurately. A better fit is found by re-evaluating the model.

The Helmholtz model that was derived in Section 3.1 was based on a number of assumptions. Because the model and the experimental data do not match, it is possible that some of the assumptions used may be invalid or inaccurate. There are two aspects of the model that do not fit the data; the magnitude of the resonance and the frequency of the resonance. The mass and stiffness of the system primarily affect the frequency of the resonance. The stiffness of the system is a function of physical parameters that cannot be changed. The mass of the system is a function of physical parameters that can be evaluated for change. The effective leak length was discussed in 3.1.

$$L' = L + 1.4a$$

Equation 3-3

Kinsler and Frey show the effective leak length to be a linear function of the radius of the opening. This leak length is then used to calculate the mass of the fluid oscillating within the leak. In order to match the resonant frequencies, the coefficient acting on the radius of the leak was varied. The results are shown in Figure 4.7.

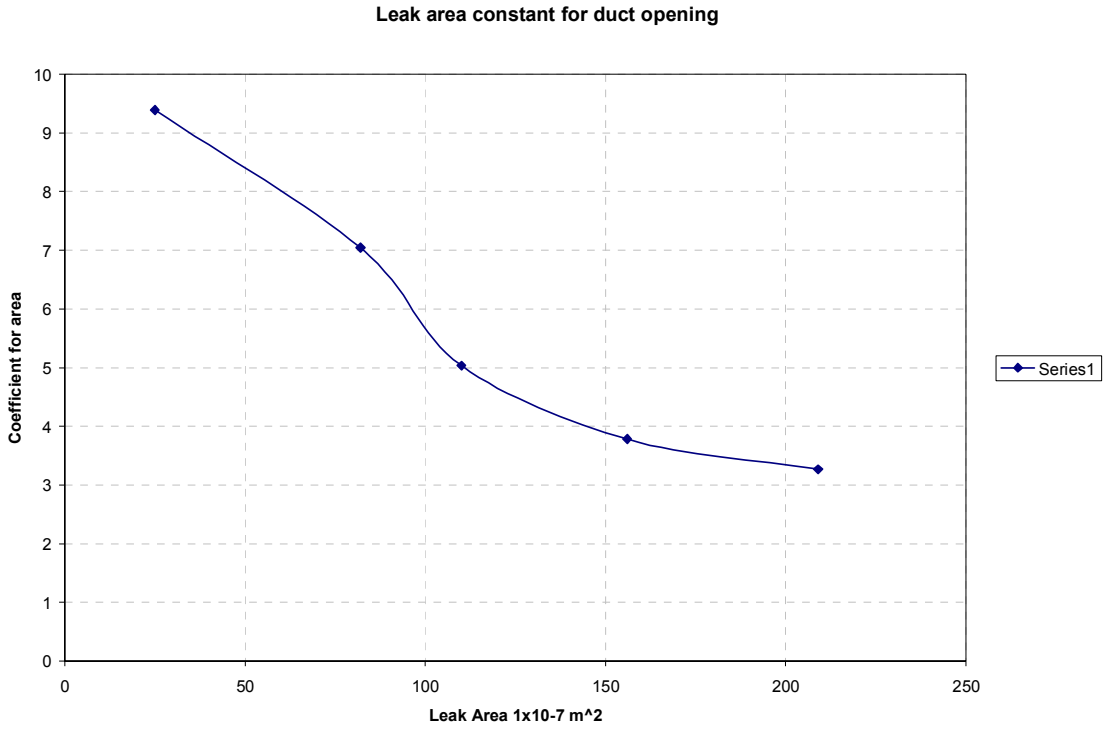

Figure 4.7: Leak area constant as a function of leak area

Figure 4.7 suggests that there is a functional relationship between the area of the leak, and the coefficient for the radius. From a qualitative point of view, it makes sense that the effective leak length would decrease as the leak area increases. As the leak area increases, the slug of fluid is allowed to move more freely, and dissipate momentum more quickly. A small leak has higher viscous losses and higher internal velocities. A higher fluid velocity takes more time to dissipate its momentum to the surrounding fluid. This causes an effectively larger slug of fluid, and thus a larger effective leak length.

The absorption coefficient in the damping term is built around the previously stated assumptions. Instead of re-deriving the absorption coefficient, a correction factor, Ω, was added to Equation 3-6. This can be seen as Equation 4-1.

$$\alpha_w = \frac{\Omega}{ac}\left(\frac{\eta\omega}{2\rho_o}\right)^{1/2}\left(1+\frac{\gamma-1}{\sqrt{\mathrm{Pr}}}\right) \quad \left(1/m\right)$$

Equation 4-1

A correction factor of 2.5 provided nearly perfect damping to match the data. It is important to note that as Ω increases, the absorption coefficient increases. While the resonant frequency is a function of damping and mass, it turned out that only the mass term really had an effect on changing the frequency of the resonance. The newly matched models can be seen in Figure 4.8 (HAL-1M2-F-156).

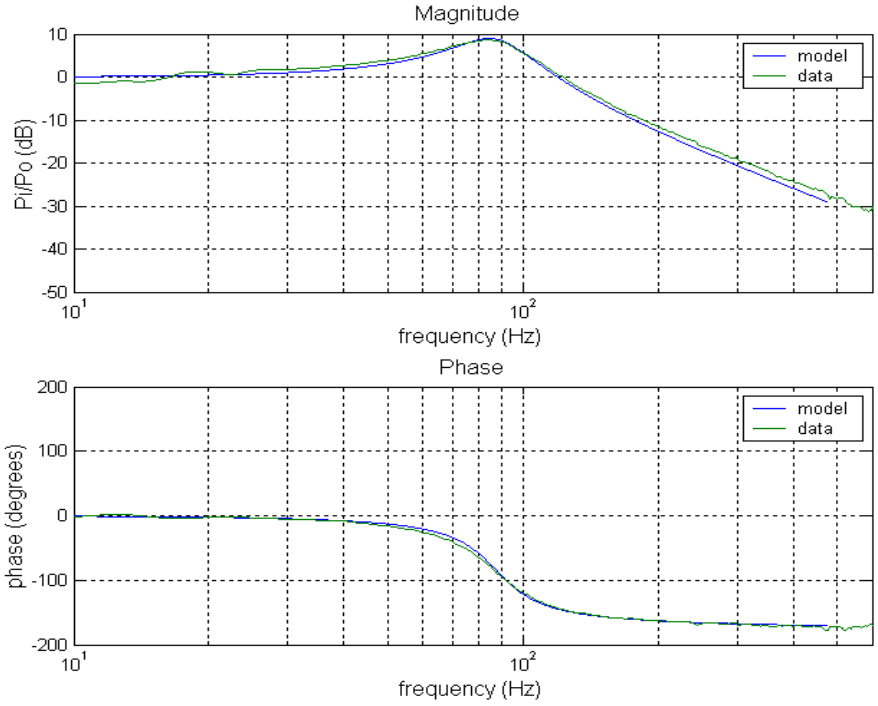

Figure 4.8: ¾" leak compared to the corrected model

Matching the model to the data provides a clear demonstration that the Helmholtz resonance exists in the ear cup. The noise below 30 Hz is due to poor coherence between the microphones.

4.2 Piston Resonance Testing

It was discussed earlier that the piston resonance, and its effect on hearing protection, has been well documented over the years. Even though this is the case, testing for the piston resonance is not a redundant exercise. Research has not been previously documented where both the piston resonance and Helmholtz resonance are assumed to be present within the ear cup. It has been shown that a leak introduced to the ear cup will initiate a Helmholtz resonance. Prior researchers have under emphasized the leak, and may not have designed the experiments carefully enough to exclude the leak. The results of these tests show that the piston resonance occurs over 100 Hz higher than the Helmholtz resonance.

4.2.1 Experimental Set Up

The purpose of the piston testing is to isolate the mechanical resonance of the ear cup on the seal. More specifically, the goal of this experiment to isolate the ear cup vibration along the axis perpendicular to the plane of the ear. The piston resonance is the lowest frequency dynamic of the mechanical vibrations. This means that it is not necessary to secure the ear cup in multiple locations to isolate other instances of mechanical vibration.

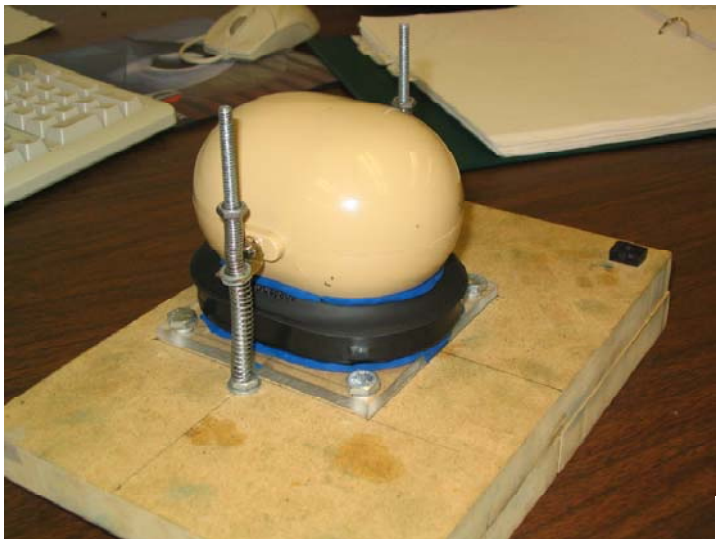

Figure 4.9: Picture of piston testing set up

The test rig used for the Helmholtz testing was used to secure the ear cup for the piston testing, seen in Figure 4.9. It is also necessary to eliminate any leaks that expose the inner cavity of the ear cup to the ambient. Sealing the mating surfaces between the ear seal and the ear cup with putty minimized the leaks. The blue material seen in Figure 4.9 is the putty that was used. Along with sealing the leak, it is also important to ensure that the different seal materials have the same force exerted on them.

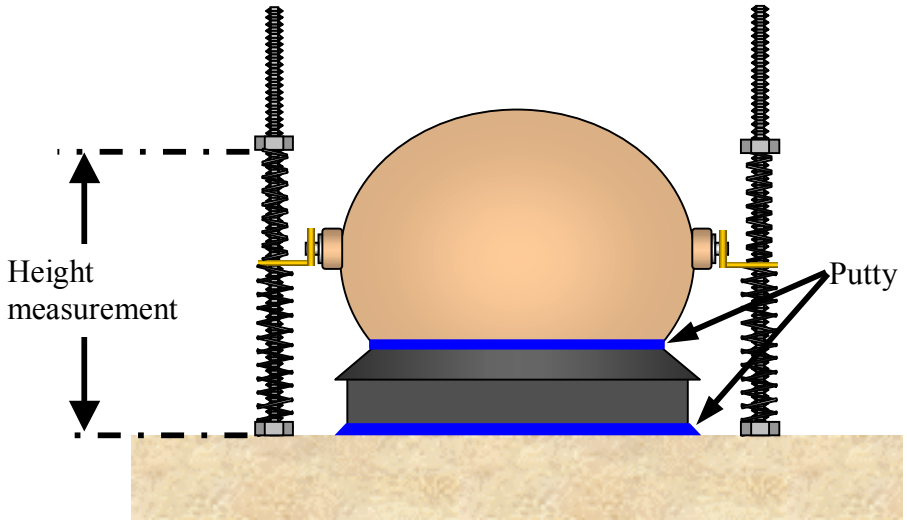

Figure 4.10: Schematic of height adjustment for ear seals

Knowing the precise amount of load acting on the ear cup is not as important as making sure the force exerted from test to test is the same. A means of attaining constant force was found by measuring the distance between the base of the test rig to the bottom of the spring tension nut. This can be seen in Figure 4.10. This height adjustment was used for the grey foam seal and the DCCI undercut seal. The piston tests involving the stiff gasket material were conducted with the spring tension nuts screwed down as far as they would go.

The piston resonance tests were conducted in a reverberant chamber, with a noise source in one corner of the room and the ear cup near the center of the room. A reference microphone was placed just outside the ear cup, and a microphone was placed inside the ear cup. Appendix A contains the serial number coding for these tests.

4.2.2 Test Results

The piston resonance was identified to occur around 400 Hz for the different seal materials used. The grey seal, DCCI undercut seal and stiff gasket seal were the three seals used in the piston resonance tests. All three exhibited different DC gains, resonant gains and resonant frequencies.

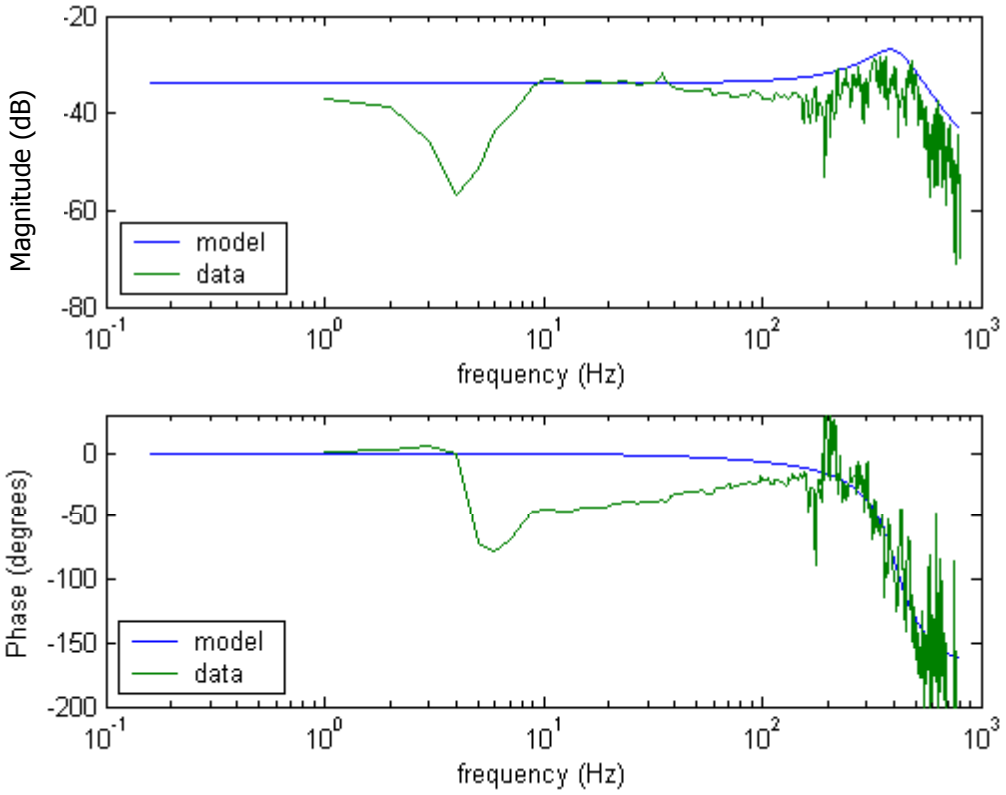

Figure 4.11: Grey seal piston resonance compared to model

The piston response data is not as clear as the Helmholtz data. The resonance is more easily identified when it is compared to the model, as seen in Figure 4.11 (NGAR-1M3-F-PUT). The spring constant of the data was calibrated until a good fit was found between the model and the data. For the grey seal, the spring constant was approximated as 130000 N/m. The relative damping and stiffness values of the seals compared to one another are of interest within the scope of this experiment, not the actual values of this parameter. Figure 4.11 shows that the model captures the dynamics of the piston resonance.

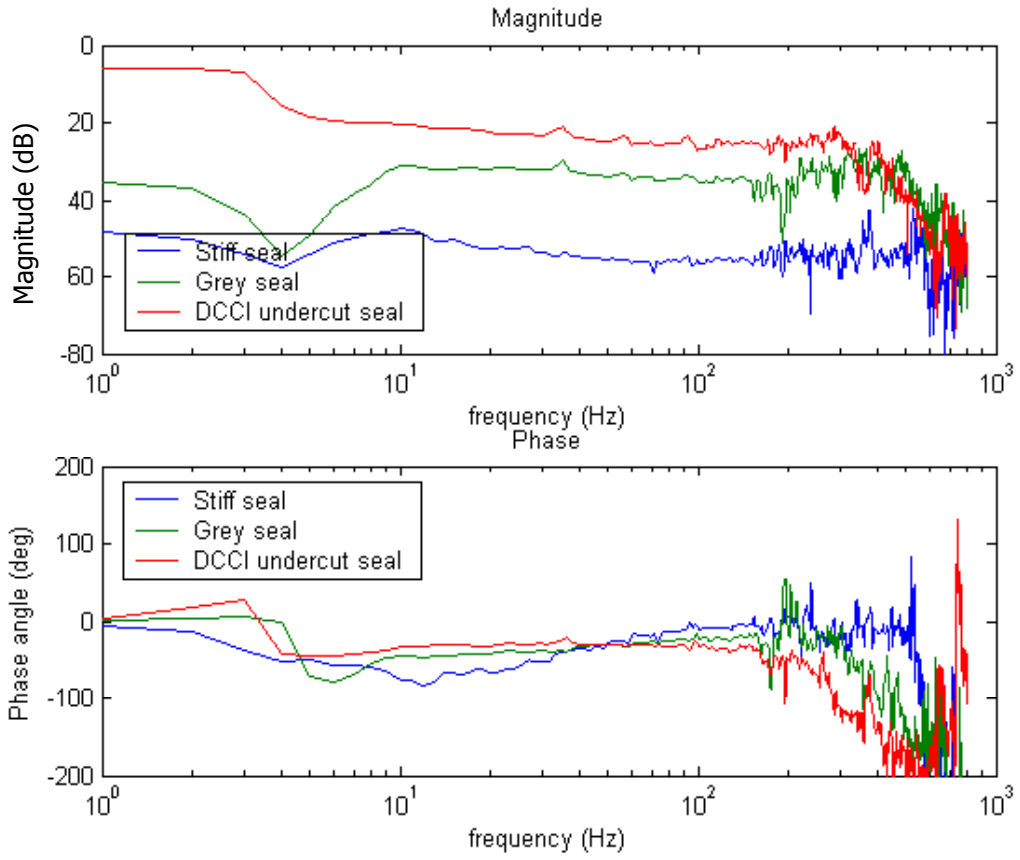

Figure 4.12: No leak comparison of different seal materials

Figure 4.12 (NVAR-1M5-F, NGAR-1M3-F-PUT, NSAR-1M3-F-NEW) is a comparison of the piston response for the three different seals. This comparison exhibits trends that are consistent with what the piston model predicts. The only variable changing in these experiments is the seal material. The rubber gasket appears much stiffer than the grey seal and the DCCI undercut seal, and thus was expected to exhibit more attenuation before resonance. Qualitatively, the grey seal and the DCCI undercut seal feel similar in their stiffness, so it was difficult to predict their relative stiffness to one another. Figure 4.12 indicates that the grey seal is stiffer than the DCCI undercut seal as the grey seal has better low frequency attenuation and a higher resonant frequency. The values of seal stiffness as predicted by the calibrated model are shown below.

Table 4-2 : Seal stiffness values

Seal Material	Stiffness as predicted by the model (N/m)
DCCI undercut seal	**60000**
Grey seal	**130000**
Rubber gasket seal	**1200000**

As mentioned before, the seal stiffness values shown in

Table 4-2 are not the actual stiffness values of the seals. What is important to notice is the relative difference between the stiffness values. Doubling the stiffness of the seal provides nearly 15 dB of noise attenuation as seen in Figure 4.12. Increasing stiffness by a factor of 10 increases the attenuation of the ear cup by another 20 dB. This shows that increasing seal stiffness is an effective way of attenuating noise contributed by the piston resonance.

4.3 Coupled Response Testing

The data highlighted in this section shows the coupled response of the piston and Helmholtz resonances. The first set of tests was conducted on a bench top, and the results clearly capture the two resonances. The second set of tests was conducted with the ear cup mounted on a head. The results of these tests do not show the separate resonances as clearly as the bench top tests.

4.3.1 Experimental Set Up (Bench Top)

The first set of tests was conducted on the bench top using the same test rig used for the piston and Helmholtz tests. The same seals used in the piston tests, DCCI undercut, grey and rubber gasket, were used in the coupled testing. Copper tubing was used to create a known leak for all the seals. All of the coupled tests were conducted in a reverberation chamber.

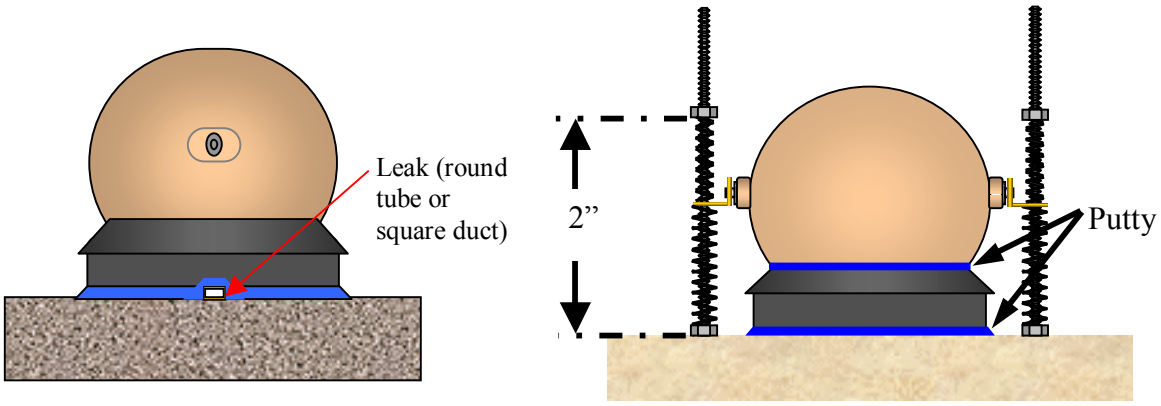

Figure 4.13: Test configuration of coupled response bench tests

Figure 4.13 is an illustration of the test configuration used for the coupled response tests. A copper tube was placed underneath the seal in order to create a known leak. The dimensions of the copper tubing can be seen in Table 4-3 below. The area around the leak and the seal was sealed up with putty. The test rig was set at a height of 2” for the coupled tests involving the grey and DCCI undercut seal. The tests with the stiff gasket seal were conducted with the test rig tightened down as far as possible. Similar to the prior tests, a reference microphone was placed just outside the leak, and a signal microphone was placed in the center of the ear cup.

Table 4-3: Tube dimensions used for coupled response testing

Tube	Inner Diameter (m)	Area (m^2 x10^{-7})	Leak Length (m)
	.00167 x .00401	67.27	.01927
	.00139	61.31	.0185
	.00226	160.54	.01917
	.00307	296.74	.01922

4.3.2 Experimental Set Up (On the Head)

The second set of tests performed for the coupled response measurements were on a head. The ear cup was placed in the headband with a microphone inside the ear cup, and one at the exterior bottom of the ear cup.

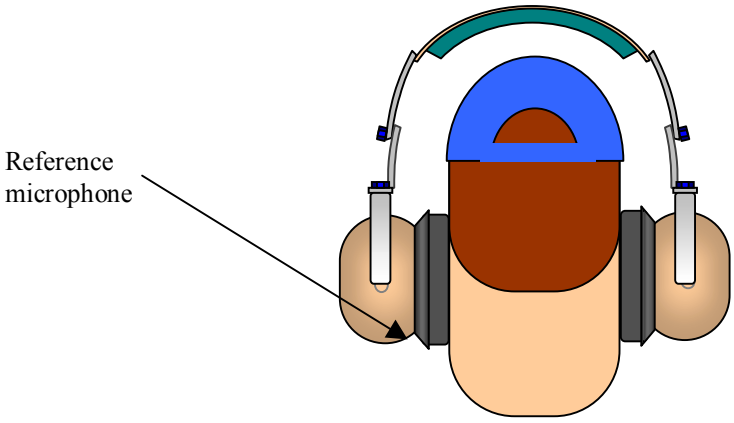

Figure 4.14: Test configuration for on the head coupled experiment

Figure 4.14 is an illustration of the test configuration for the on-head testing of the coupled response. The DCCI undercut seal and the grey seal were used for these tests. A no seal case was used instead of the gasket material. This was done because it was difficult to mount the gasket material to the cup while it was mounted on the head. These tests were conducted inside the reverberation chamber to simulate a more realistic noise field. No artificial leaks were introduced to the ear cup with any of the seals for this test

scenario. This test was intended to measure the actual attenuation a user would experience with the ear cup.

4.3.3 Bench Top Coupled Response Results

For the first set of tests, a leak size of 160e-7 m^2 was chosen. The first step in testing was to compare how well the experimental data matched the model.

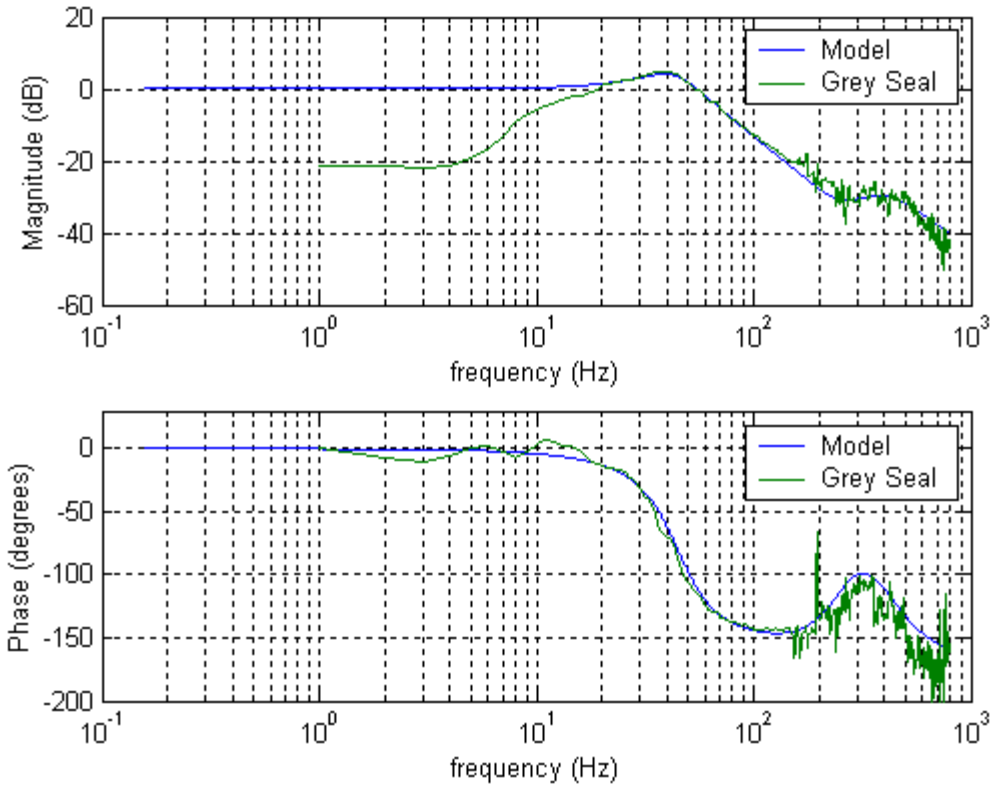

Figure 4.15: Model compared to grey seal with 160x10^{-7} m^2 leak

Figure 4.15 (FXAR-1M3-F-160new) is a comparison between the experimental data, and the coupled model. The stiffness value of the grey seal was 130000 N/m, the same as found earlier in the piston resonance tests. The Helmholtz resonance distinctly occurs at 40 Hz. This is 40 Hz lower than the Helmholtz resonance for the 156e-7 m^2 leak. The Helmholtz leak in the prior tests was ¼" shorter than the tube length used for this test. In the case of the coupled response, a longer leak length corresponds to a higher mass of air within the leak. This contributes to a lower resonant frequency. The piston resonance

distinctly occurs at 350 Hz. This is the same frequency as tested in the piston resonance section.

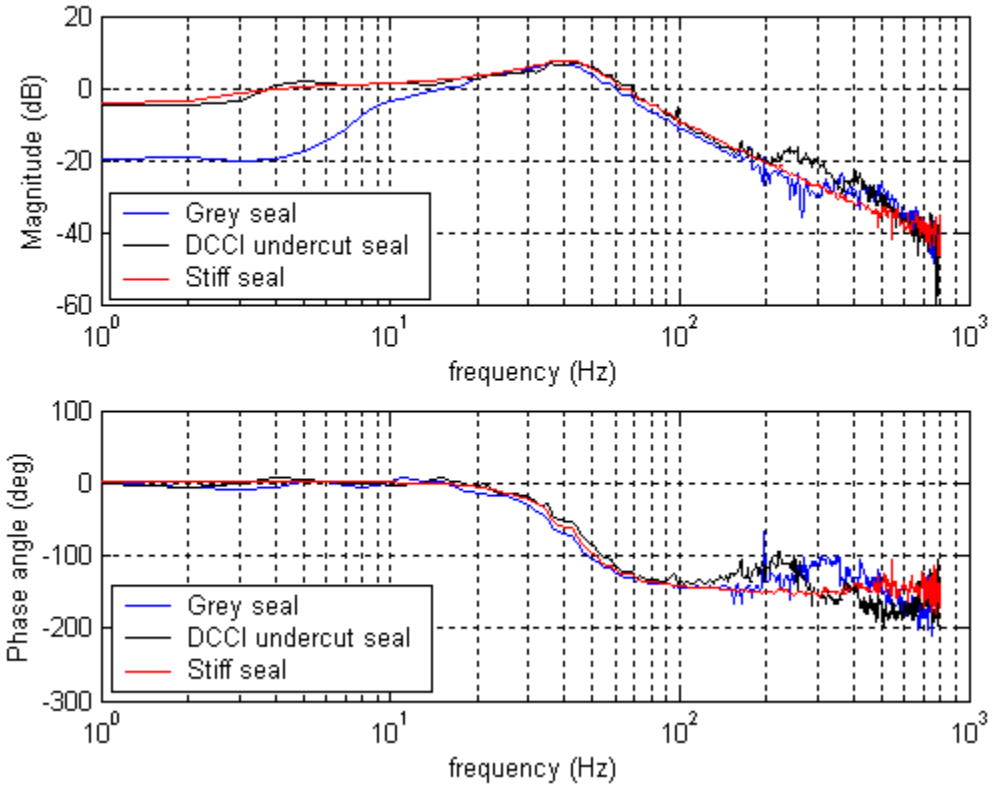

Figure 4.16: Seal comparison for a circular leak of 160 x 10^{-7} m^2

Figure 4.16 (FXAR-1M3-F-160new, HAR-1M3-F-160, FVAR-1M5-F-160) is a comparison of the coupled response of the three different seals. Each seal has a leak area of 160e-7 m^2. For the stiff seal test, the copper tube was used instead of cutting out a section of the gasket in order to remedy the discrepancy between the resonant frequency of the previous Helmholtz test, and the coupled response tests. With all the seals sharing the same leak, the Helmholtz resonance occurs at nearly 40 Hz for all three cases. The three seals exhibit nearly the same response above 10 Hz, and below 200 Hz. Above 200 Hz, the stiffness of the seals controls the behavior of the frequency response. Similar to the results seen in the piston resonance section, the DCCI undercut seal has the lowest resonant frequency, followed by the grey seal. The gasket seal does not seem to have a piston resonance below 800 Hz.

4.3.4 On the Head Coupled Test Results

The expectation for the on-head testing was to see a large contribution from the Helmholtz resonance that would outweigh any contribution made by the piston resonance. In the three seal configurations used for this test scenario, this was not found to be the case.

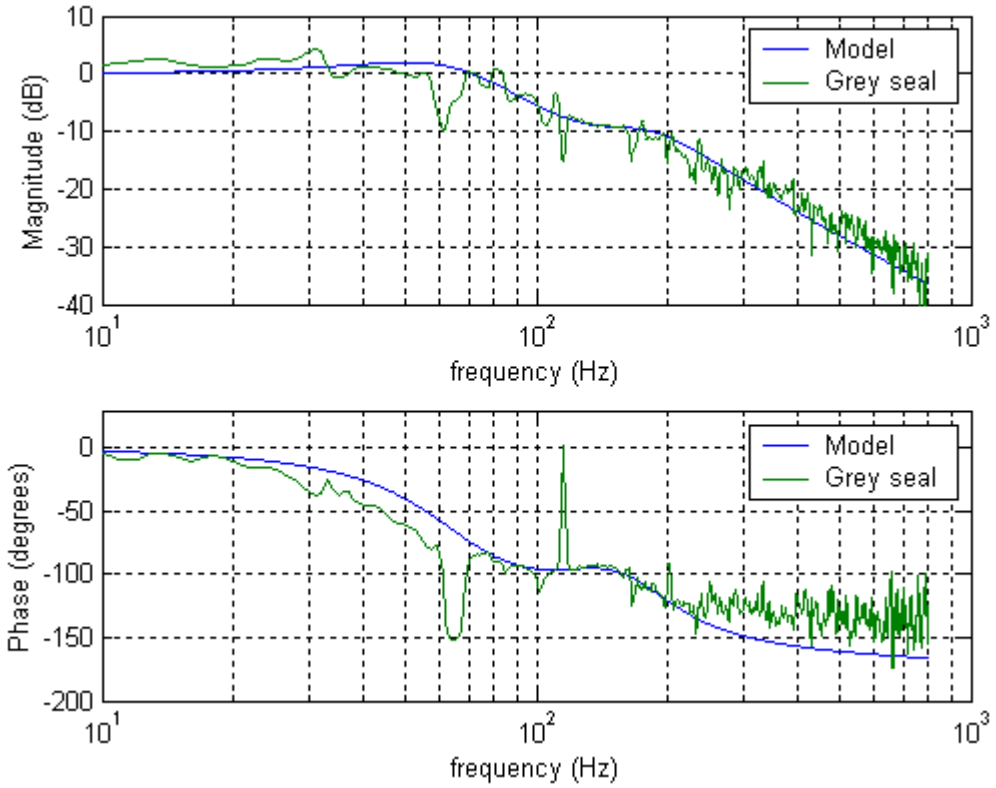

Figure 4.17: Grey foam seal on the head compared to coupled model

Figure 4.17 (JGAR-1M5-F-#2) is the result of the grey seal coupled on-head test. The data is compared to the coupled model. The leak area, leak length, effective seal damping and effective seal stiffness are unknown in this test. These values were found by calibrating the model to the data as closely as possible. It is convenient to separate the data into the Helmholtz resonance, and the piston resonance. In order to match the Helmholtz resonance to the model, the leak area was estimated to be 180 x 10^{-7} m^2. The damping of the Helmholtz resonance was also higher. A correction factor of 3.4 was

used, as opposed to the correction factor of 2.5 used in the previous Helmholtz tests. The increased correction factor may be due to increased damping caused by numerous small leaks. The previous Helmholtz tests only took a single leak into account. A look at the piston resonance reveals more changes. The flesh on the head has stiffness and damping properties that will contribute to the total stiffness and damping of the entire system. In this case, the effective stiffness of the system was found to be 23000 N/m. The grey seal has a stiffness of 130000 N/m, which translates to a skin stiffness of approximately 28000 N/m. The damping value of the seal was also reduced. The piston tests for the grey seal revealed a damping value of 20 kg/s. The effective damping of the coupled on-head model is 16 kg/s.

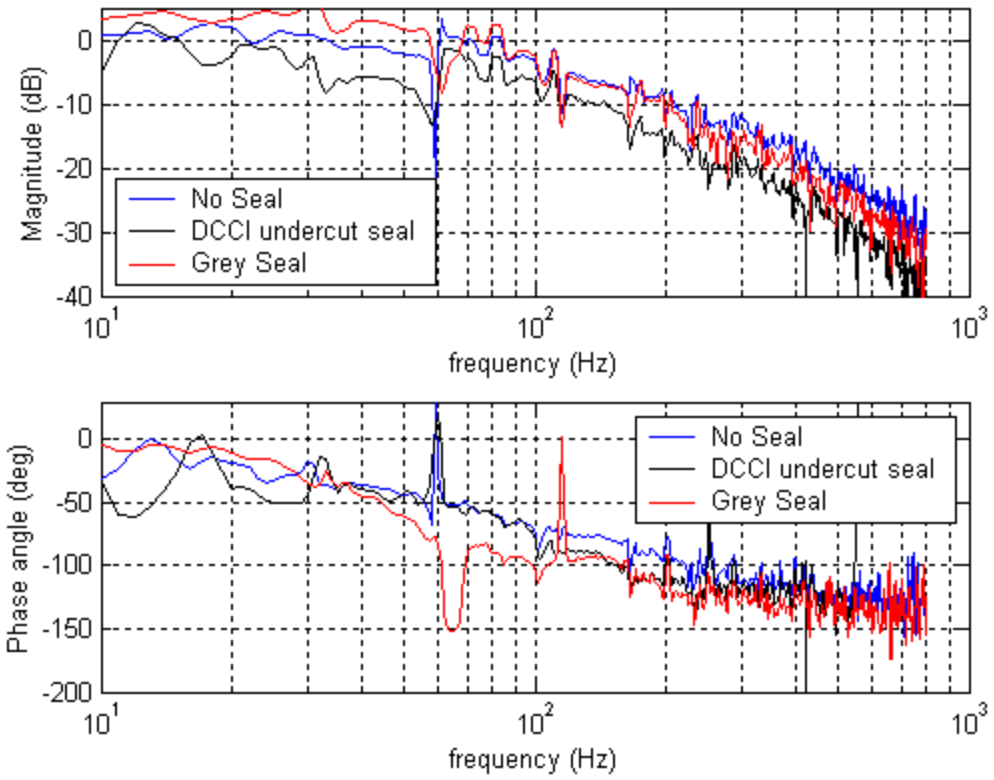

Figure 4.18: On the head test comparison

Figure 4.18 (JAR-1M5-F, JVAR-1M5-F-2, JGAR-1M5-F-#2) is a comparison of the three seals used for the on-head coupled testing. The results shown in Figure 4.18 show attenuation levels contrary to the results of the piston tests. The no-seal, or stiff-seal case showed the best attenuation in the piston tests, whereas in this test, it exhibits

the worst attenuation. In contrast, the DCCI undercut seal showed poor attenuation on the bench, but on the head, it outperforms the other two seals. The stiffness of these three seals is limited by the stiffness of the skin. This means that when the ear cups are mounted on the head, the effective stiffness of the seals is all very nearly 23000 N/m. Given that the seals have the same stiffness values for the on-head coupled tests, another parameter must be affecting the attenuation. In calibrating the model to fit the data, it was found that the differences in attenuation could be attributed to different leak areas. In fitting the model to the data, it was found that the DCCI seal had the smallest leak area, while the no-seal case had the highest leak area.

4.4 Low Frequency Effects of a Foam Insert

Nearly all hearing protectors have a foam insert inside the cup. This insert is generally used to attenuate high frequency noise. The purpose of this testing is to see whether the foam insert affects low frequency dynamics. This section examines the effects of a foam insert inside the ear cup for the Helmholtz resonance, and the coupled on-head tests.

The foam does not absorb much of the bulk mode energy, therefore it is expected that the low frequency dynamics will be similar with or without the foam insert. Figure 4.19 compares the Helmholtz resonance of a case with and without the foam insert.

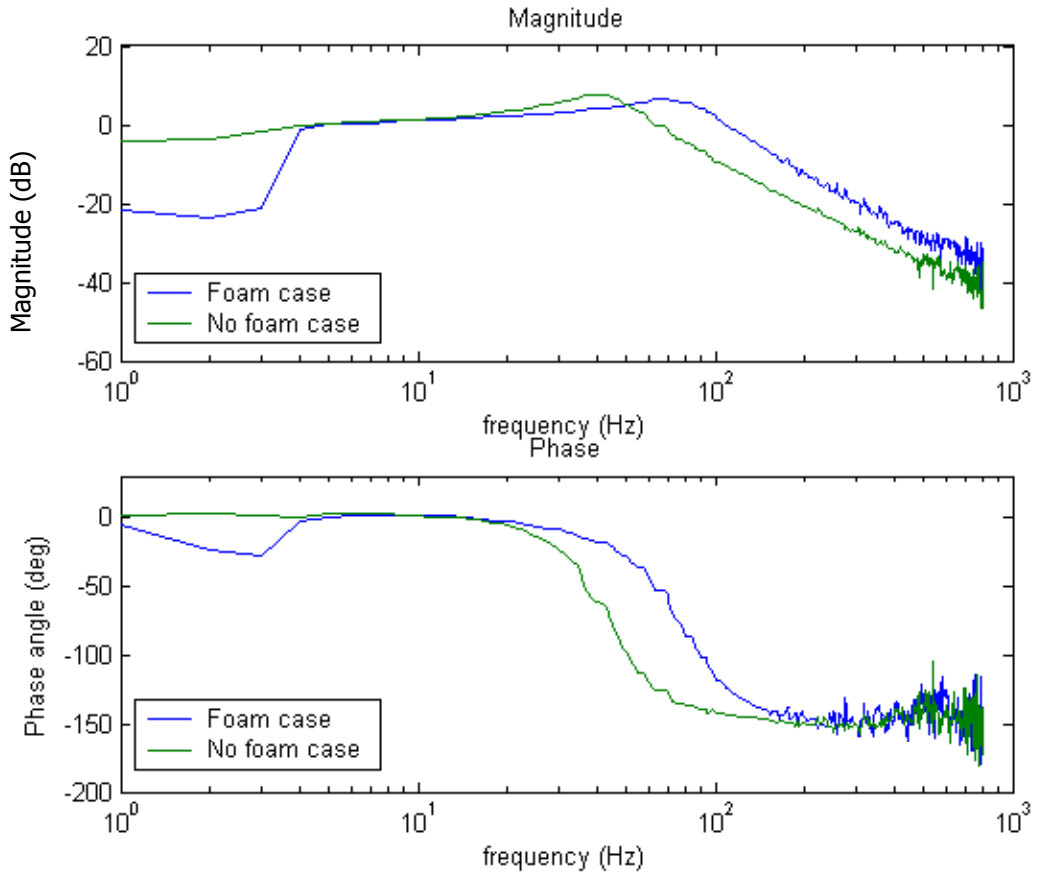

Figure 4.19: Foam insert compared to no insert for a 156×10^{-7} m^2 leak area

The results of Figure 4.19 do not agree with the contention that the foam insert will not affect the response of the Helmholtz resonance. The magnitudes of the two peaks are just

about the same. A larger leak size would produce higher amplitude along with a higher resonant frequency. Instead, this trend corresponds more closely to a volume change in the cup. The foam is displacing volume in the cup, and therefore increasing the stiffness of the air spring. This volume change caused 50 Hz frequency change, but did not attenuate the system at all. In section 3.1.1, it was discussed that a volume decrease would lead to an increase in the resonant frequency, and an increase in the resonant gain. In this case, an increase in the resonant frequency occurred, but there was no increase in the resonant gain. This suggests that the foam absorbed some of the energy of the Helmholtz resonance, and does have an effect on the low frequency dynamics.

The next case to look at is the foam insert on the head. This test was conducted in the same manner as the other on-head data tests. In this case, the foam insert was placed in the cup with the signal microphone near the ear.

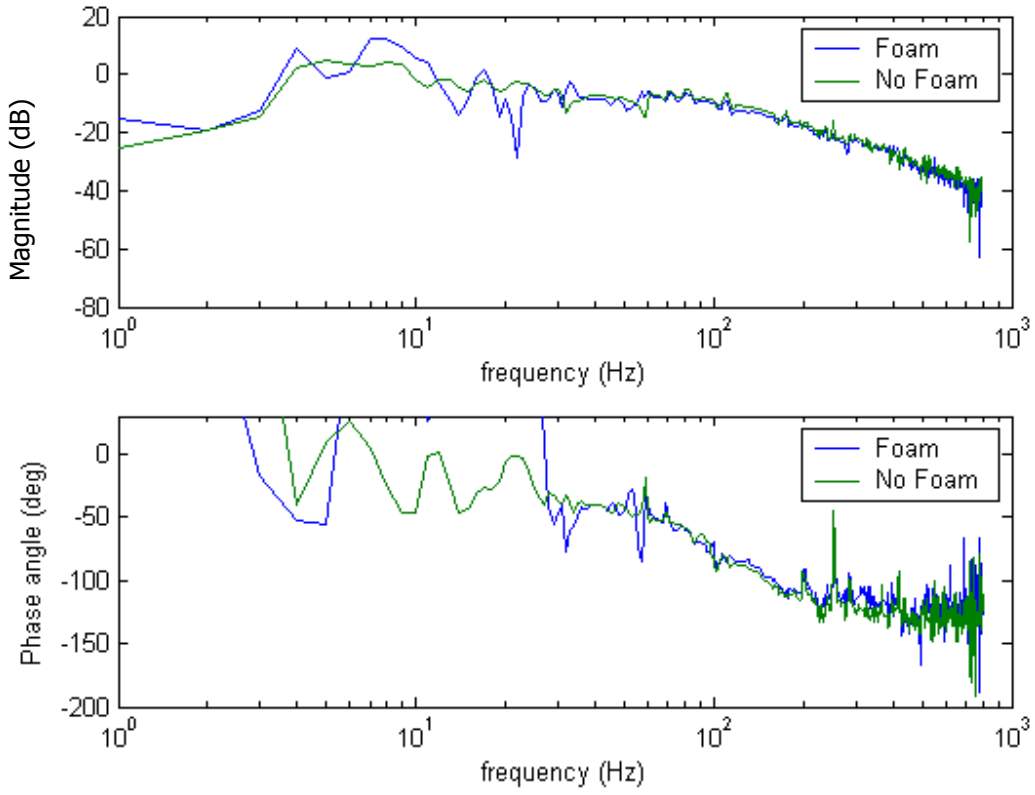

Figure 4.20: Head data with foam insert compared to head data with no insert

Unlike Figure 4.19, Figure 4.20 does not show an increase in resonant frequency. This is an encouraging result, because it means that the foam does not affect the low frequency performance of the cup during its intended use.

4.5 Acoustic Mode Shapes

The DCCI cup has three primary directions for mode shapes to set up. If the head cup were a box, the mode analysis would be straightforward. In a box, the modes have a distinct dimensional length to set up in. This means that there is one specific frequency that corresponds to one specific mode. The near spherical shape of the DCCI cup makes mode frequency prediction more difficult due to three dimensional mode coupling. In spite of this, the first few mode shapes are still relatively easy to predict and identify. This section discusses the procedure for predicting and identifying the first six acoustic modes of the DCCI cup.

For the first analysis of a standing wave, consider a closed – closed tube. In order for a standing wave to exist in this environment, the velocity of the wave is assumed to be zero at the boundaries. When the velocity is zero, the pressure of the wave is at a maximum. This can be seen in Figure 4.21.

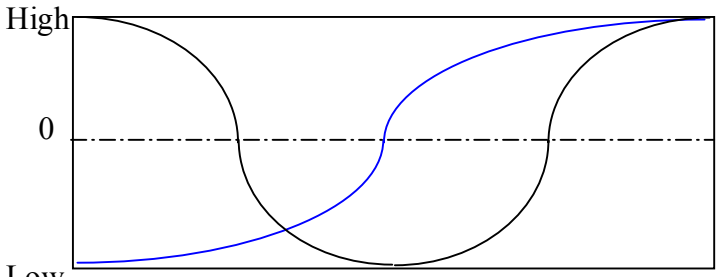

Figure 4.21: Mode shapes in a closed - closed tube

The frequencies that set up in a given length are easily found using a simple relationship found in Equation 4-2.

$$\lambda = \frac{c}{f}$$

Equation 4-2

The variable λ is the wavelength in meters, c is the speed of sound in m/s and f is the frequency in (1/s). Equation 4-2 in its current form will only predict the dimensions that full waves will set up in. Due to the boundary conditions of a closed- closed tube, only

waves that have a maximum absolute pressure at the walls can exist. This means that Equation 4-2 can be modified.

$$f = .5x * \frac{c}{\lambda}$$

Equation 4-3

The variable x is any scalar multiple greater than or equal to one. Equation 4-3 can be used to predict the frequency of any given standing wave that will occur in any given dimension of the cup. As mentioned earlier, Equation 4-3 can only be used to get a good idea as to where any standing wave will be. This is due to the near spherical geometry of the head cup. Along any given axis of the cup, there is no one length that a standing wave will set up in. Instead, the effective length will be a summation of all the lengths in the axis. This will be the corresponding length that a standing wave will occur.

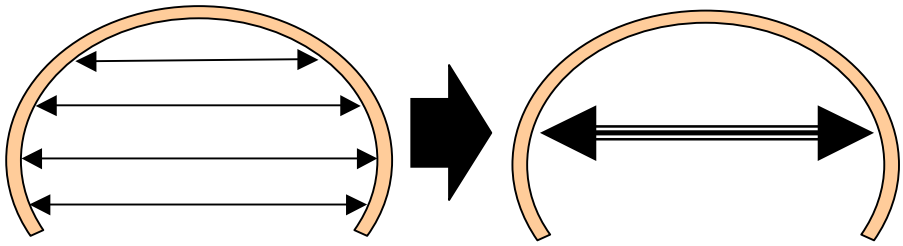

Figure 4.22: Summation of cup lengths to form effective cup length

Figure 4.22 shows how a number of different lengths sum up to give an effective cup length. Predicting the contribution of each length would be a complicated process, and would have needed to be verified by testing anyway. Instead, Equation 4-3 was used to predict the frequency range that the standing wave would set up in, and the actual frequency was found with testing.

4.5.1 Experimental Set Up

The process of finding the standing waves begins with taking an FRF between the source and a signal microphone inside the cup. The FRF is taken in the frequency range that the mode is predicted to be found in. Once found, the process of identifying the mode begins. Figure 4.21 shows the pressure along the mode shape changes spatially. Along with varying pressure, the phase of the mode also changes spatially. Placing a

microphone along the axis of the mode, and moving it along the axis, will provide the necessary information to identify a mode shape.

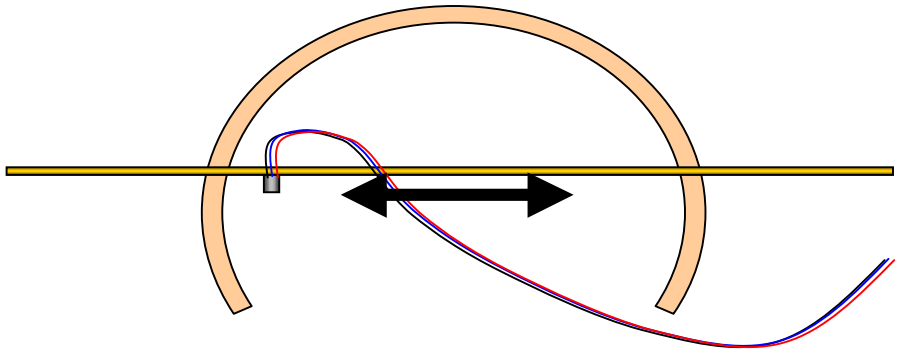

Figure 4.23: Diagram of microphone positioning

Figure 4.23 illustrates the method used to move the microphone through the path of the mode shape. This method is also used to find the mode shapes in the vertical and width directions of the cup. In order to get meaningful data, an FRF between the source and the signal microphone must be taken. This is taken while exciting the mode with a narrow band source centered at the resonant frequency of the mode being tested. In order to identify the modes accurately, the microphone was moved in 1/8" increments along the axis.

Figure 4.24: Picture of test set up for mode shape identification

Figure 4.24 represents the cup used to test for the mode shapes. Holes were drilled on all three axes in order to place the rod in the path of the various mode shapes.

4.5.2 Test Results

Before testing, the frequencies of the first six modes were predicted using Equation 4-3. This provided a good estimate as to where the mode shapes would occur. The next step was to take an FRF of the head cup. The reference microphone was placed just outside the leak, and the signal microphone was placed in the middle of the cup.

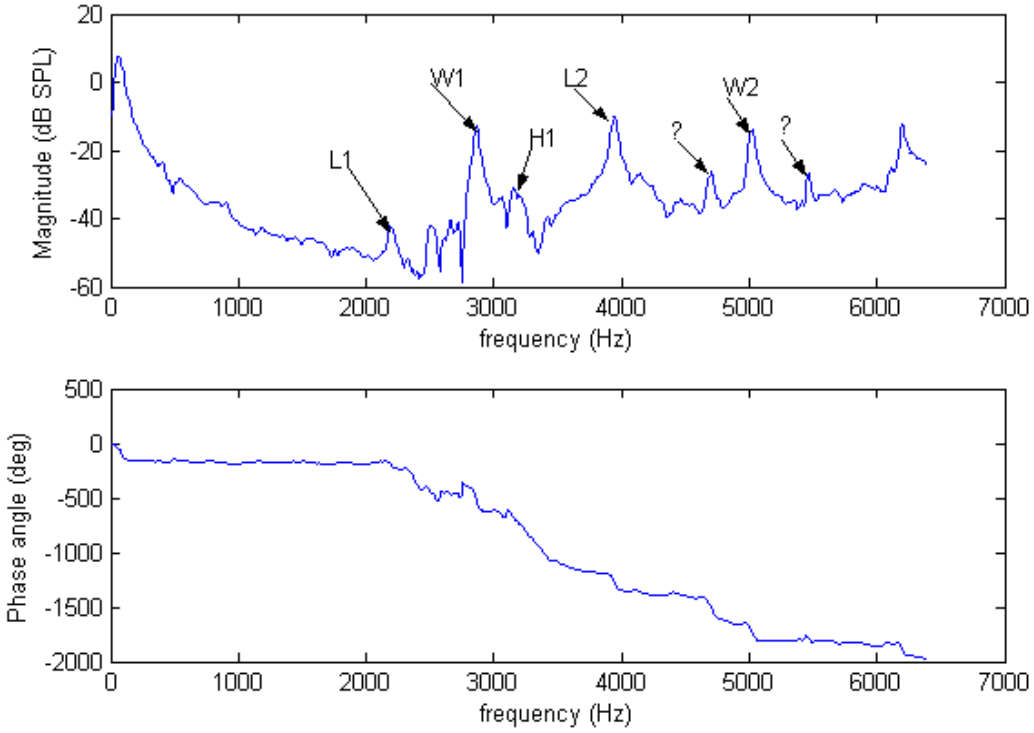

Figure 4.25: FRF of ear cup up to 6400 Hz

Figure 4.25 (HDL-1M2-F-100) is labeled with the locations of each mode. The length mode is represented by L, the width by W, and the height by H. The numbers represent a half wave (1) or a full wave (2). The peaks with question marks have not been identified due to extensive coupling of other modes in the cup.

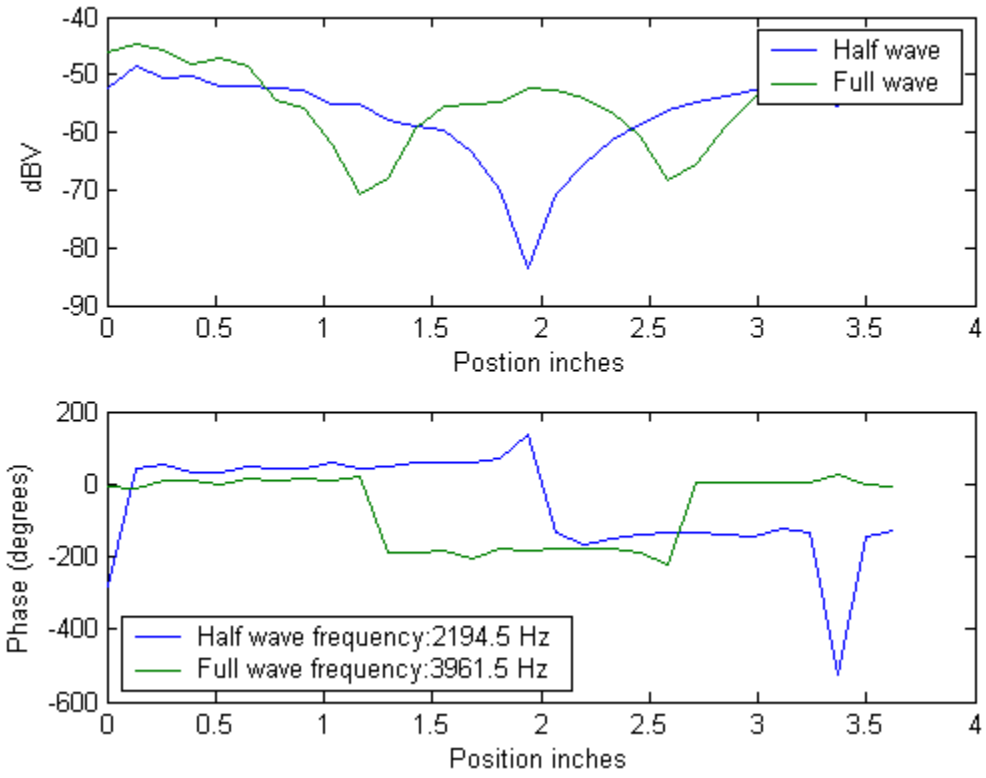

Figure 4.26: Mode shaped across length axis (L1&L2)

Figure 4.26 shows the experimental results of the first two mode shapes that occur across the length of the cup. This is the longest dimension in the cup, and thus, these standing waves occur at lowest frequencies. The first half wave occurs at 2194 Hz. The phase goes through a distinct 180-degree shift at the node of the standing wave. This is also where the magnitude of the wave is at a minimum. The full wave occurs at 3961 Hz. In a square box, the full wave would occur at twice the frequency of the half wave. In the head cup, the full wave was found to occur at 1.8 times the frequency of the half wave. The full wave is distinguishable by two 180-degree phase shifts corresponding to minimum pressure magnitudes.

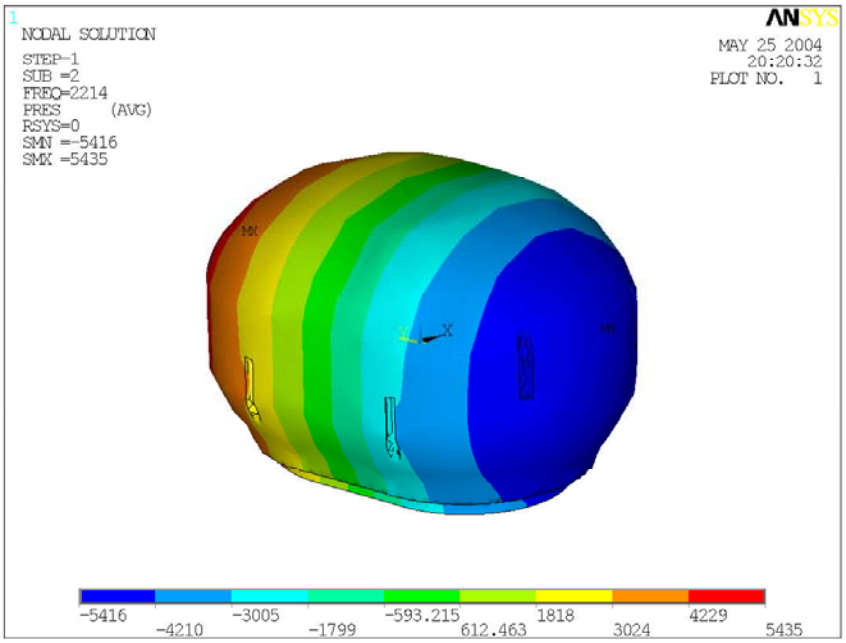

Figure 4.27: FEA results of first half wave occurring at 2214 Hz

Figure 4.27 is the result of an FE analysis of the ear cup. In this figure, the varying colors represent areas of constant pressure within the ear cup. The red area represents a high-pressure, and the blue represents a low-pressure area. The FE results provide a three-dimensional view of the pressure gradient inside the cup for different modes.

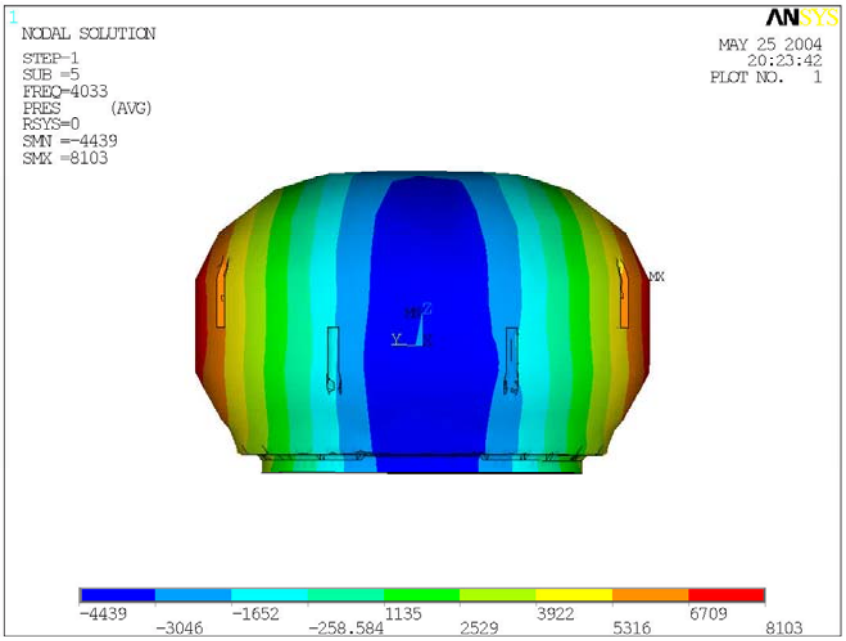

Figure 4.28: FEA results of first full wave occurring at 4033 Hz

Figure 4.28 is the FE analysis for the first full wave that occurs in the length direction of the ear cup. The previous two figures both correspond with the experimental results seen in Figure 4.26. The FE frequency predictions of the mode shapes are very close to the measured values, but the values calculated using Equation 4-3 provide very different results. A comparison of the modal frequencies of the cup can be seen in Table 4-4.

Table 4-4: Experimental, FEA and predicted modal frequencies

Frequency (tested)	FEA model frequency	Simplified Prediction	Full Wave	Half Wave	Cup dimension
2194.5	**2214**	**1758**		**X**	**Length**
3961.5	**4033**	**3516**	**X**		**Length**
2891	**2860**	**2346**		**X**	**Width**
5036.5	**5162**	**4692**	**X**		**Width**
3174.5	**3159**	**2700**		**X**	**Height**
5515.5 *	**5162**	**5401**	**X**		**Height**

* This test result yielded a half wave experimentally (Appendix B)

Table 4-4 is a comparison of the experimental modal frequencies, and the frequencies predicted by the FE analysis, and Equation 4-3. The FE analysis most closely matches the experimental results. Equation 4-3 falls short in that it does not account for the spherical shape of the ear cup. The ability to accurately predict and validate the lower frequency dynamics of the ear cup gives great cause to believe that the FE analysis can predict higher frequency dynamics of the ear cup. The remaining FE and experimental modal plots can be seen in Appendix B.

4.6 Velocity Testing

The leak has been shown to be a source term at low frequencies, but its effect at higher frequencies has yet to be determined. Section 3.1.3 makes mention of higher frequency effects of the leak as a source term. More specifically, the Bode plot of leak acceleration in Figure 3.13 shows that after the Helmholtz resonance, the acceleration of fluid within the leak does not decay with increasing frequency. If the mass of the fluid within the leak maintains a constant acceleration through higher frequencies, then the leak will continue to add energy into the cup up through higher frequencies. This set of experiments does not measure the acceleration of the fluid in the leak. The experiments are set up to measure the time integral of acceleration, i.e. velocity. In an FRF, this difference will manifest itself as a 20-dB/decade decay with increasing frequency. In this way, examining the FRF of velocity and excitation pressure will provide a reliable way of measuring the acceleration of the leak.

4.6.1 Experimental Set Up

The data taken for these tests incorporates a velocity circuit, and an exterior pressure sensor. This set up was used in order to measure the frequency response function between the fluid leak velocity and the ambient excitation pressure. The first test was designed to find the velocity of air within a leak. For this experiment, rectangular copper tubes were cut to lengths of 49.6 mm, 39.5 mm and 19.2 mm, and two holes were drilled 9.1 mm apart from centerline. Two microphones were fit into these holes, and the pipe was then fitted underneath the ear cup. This spacing allows for accurate velocity measurements up to 6300 Hz.

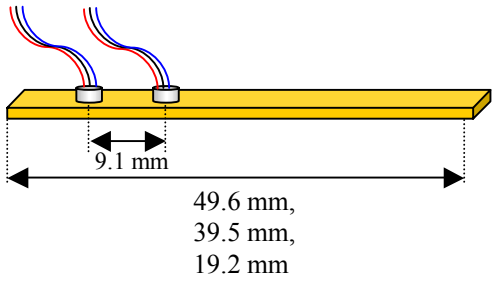

Figure 4.29: Copper tube fitted with microphones

Figure 4.29 is an illustration of the copper tube used to take the first velocity measurement. This tube was used as the leak for the cup. The stiff gasket material was used as the seal. In order to match the dimensions of the copper tube, the gasket material was layered to match the thickness of the tube.

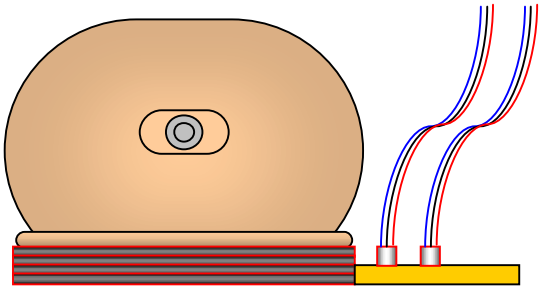

Figure 4.30: Cup with known leak and velocity probe

Figure 4.30 illustrates the experimental set up for the first set of tests performed to measure the velocity in the leak. The speaker was aimed directly at the leak in order to excite the Helmholtz resonance as efficiently as possible.

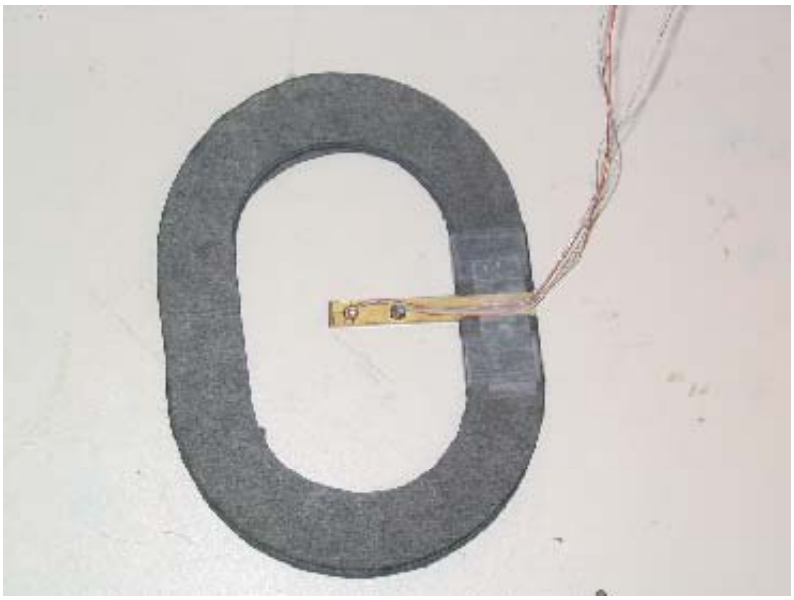

Figure 4.31: Picture of velocity probe and seal

Figure 4.31 shows the velocity-probe configured so that it fits inside the cup. The probe was then placed under the cup and excited in the same manner as the previous Helmholtz tests.

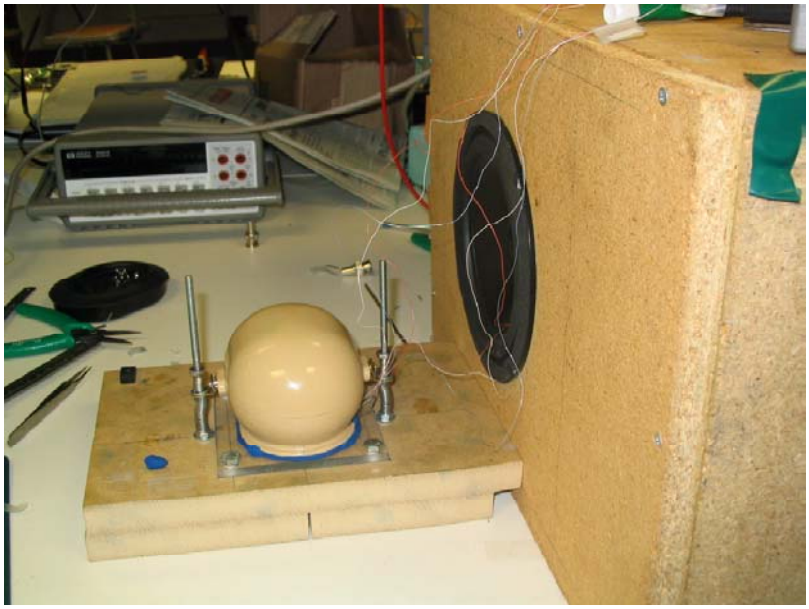

Figure 4.32: Experimental set up of velocity test

Figure 4.32 is a picture of the experimental set up used for the leak velocity tests. Putty was used around the rubber gasket, and around the leak area to remove any other leaks around the ear cup.

4.6.2 Test Results

Before testing began, it was expected that the maximum leak velocity would occur at the same frequency as the Helmholtz resonance. The testing showed this to be the case, as well as showing that the leak acceleration remains constant with frequency until 3000 Hz.

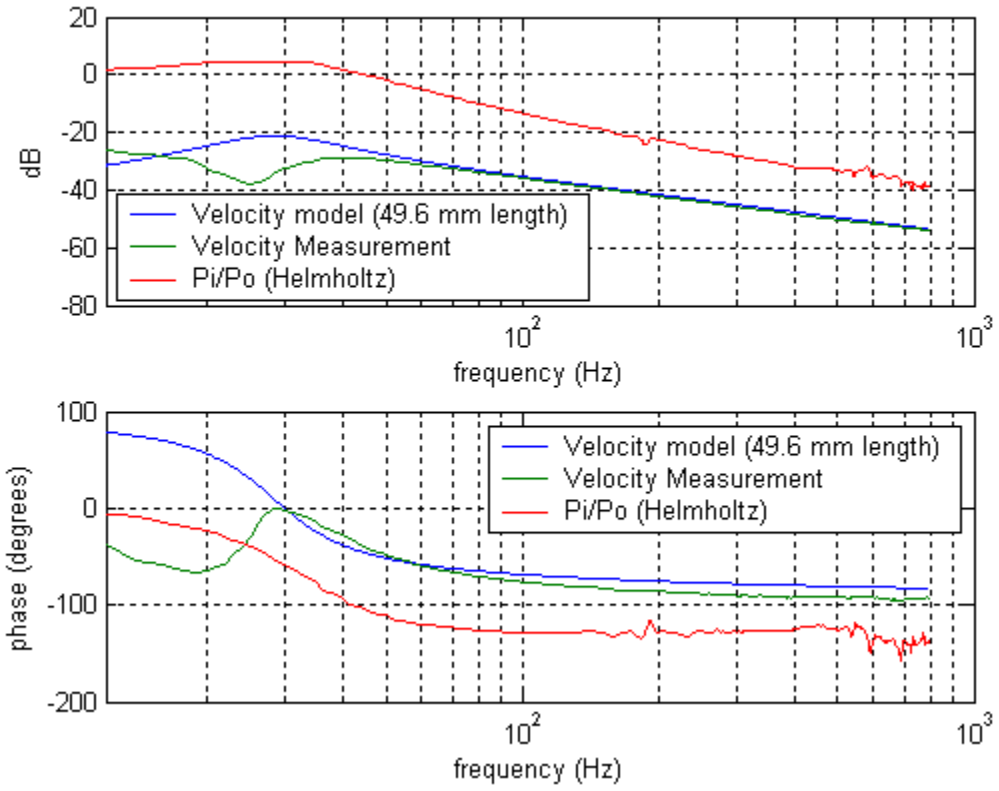

Figure 4.33: Helmholtz mode compared to leak velocity

Figure 4.33 compares the frequency response of inner pressure and ambient excitation pressure of the ear cup to the frequency response of the fluid leak velocity and ambient excitation pressure. There is a 90-degree phase difference between the velocity and pressure data. This is the expected result due to the integration of the pressure signal. The primary goal of this plot is to show that the leak velocity is maximum at the Helmholtz resonance.

The frequency response of Figure 4.33 was taken with the microphones (which will now be called the velocity probe) outside of the cup. Another test was taken with the velocity probe inside the cup under the same conditions.

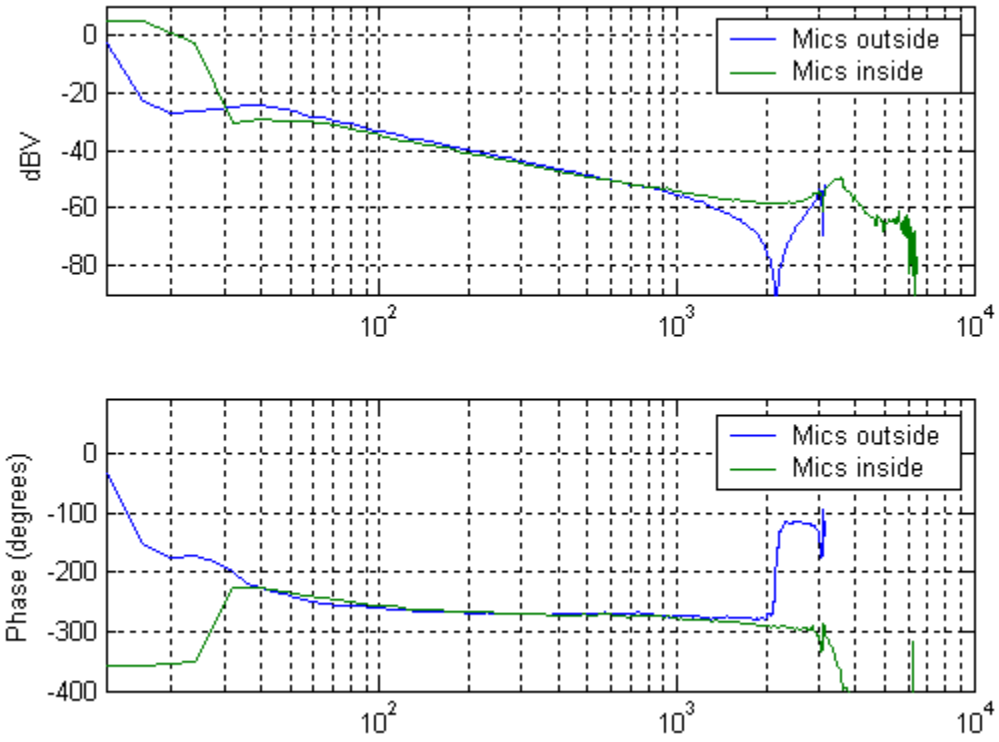

Figure 4.34: Velocity probe inside cup vs. outside cup (49.6 mm leak length)

Figure 4.34 is a comparison of the two locations of the velocity probe. The velocity-probe outside the ear cup exhibited dynamics that indicate a zero around 2000 Hz while the probe inside the cup did not. This zero could be due to a number of different factors, but it fails to show up in further tests, so it is ignored. The velocity probe inside the cup displayed a resonance around 3500 Hz. This resonance corresponds with the first half wave of the leak itself.

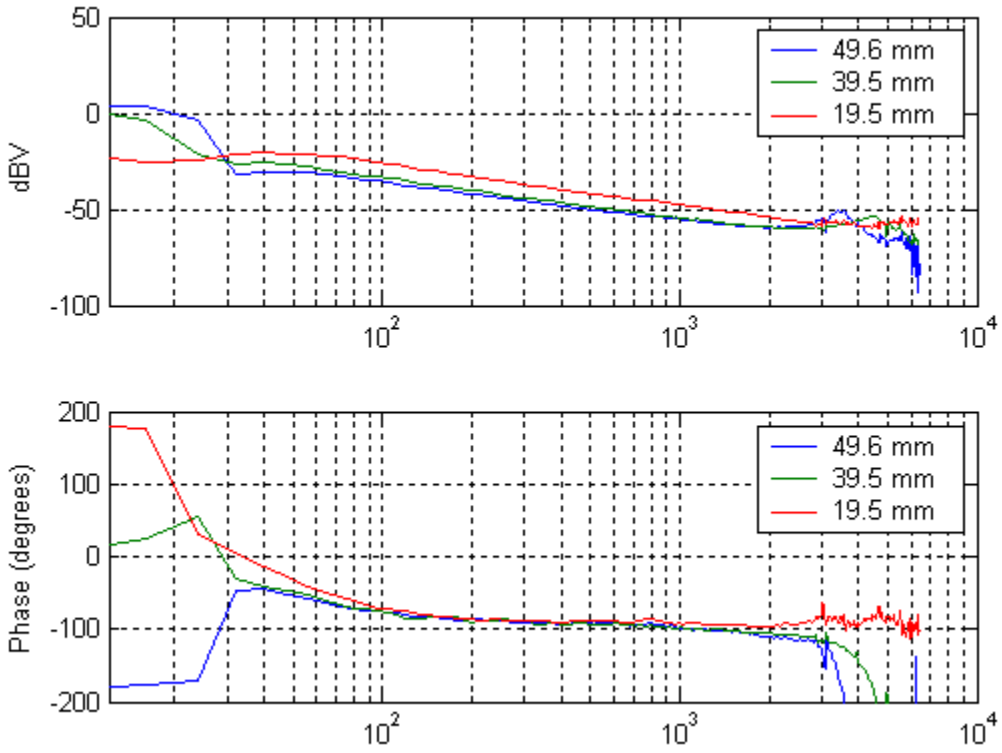

Figure 4.35: Velocity FRF of different leak lengths

Figure 4.35 is a comparison of the velocity FRF's corresponding to the different leak lengths. The two longest leaks display a duct resonance before 6300 Hz, the maximum measurable range for the velocity-probe. The shortest leak length does not show have this resonance within the range. Eliminating the duct resonance below 6300 Hz shows how long the acceleration of the fluid in the duct remains constant. The 19.5-mm duct maintains a constant 20-dB/decade decay up to 3000 Hz. This is nearly 1000 Hz higher than the other duct lengths.

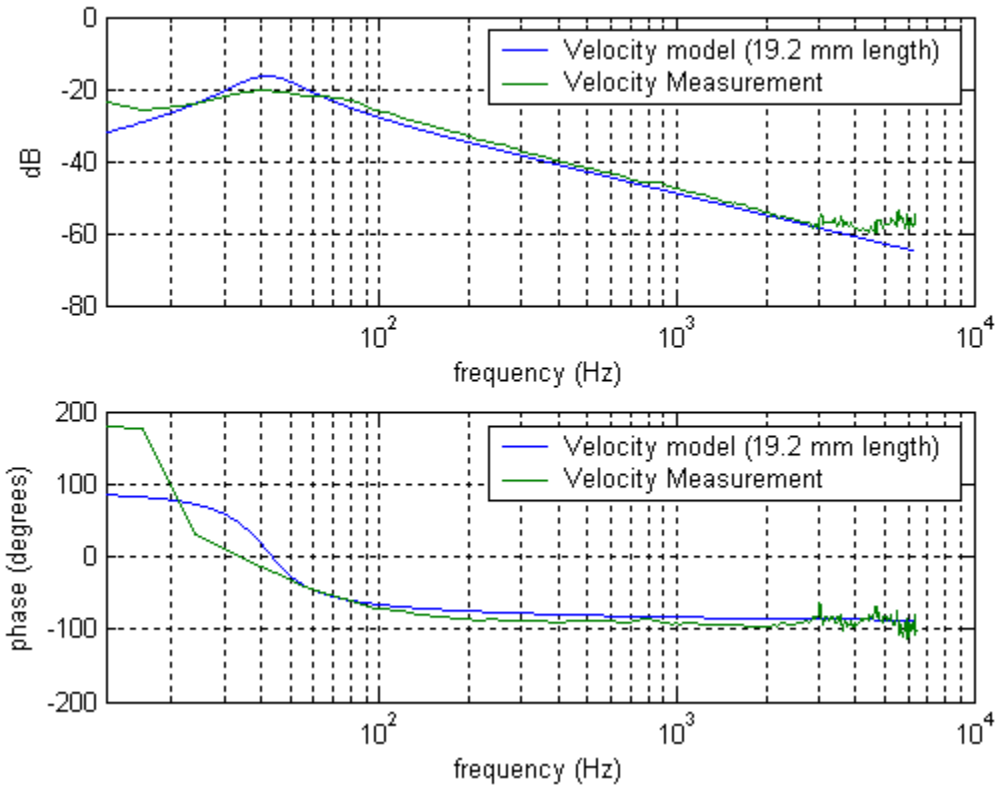

Figure 4.36: 0-6400 Hz Velocity measurement

Figure 4.36 is a comparison of the shortest leak length with the velocity model. It is evident by this plot that the acceleration of the slug of fluid within the cup is constant up to 3000 Hz. This implies that up through 3000 Hz, the Helmholtz resonance is responsible for the acceleration of fluid within the leak. Past this point, other cup dynamics become increasingly influential within the ear cup.

5 Conclusion

The goal of this research was to model and experimentally validate the mechanisms that control ear cup noise attenuation below 800 Hz. This goal was achieved by experimentally validating analytical models. The Helmholtz resonance was shown to exist, and to be a dominant dynamic effect for leak sizes as small as 25.3 e^{-7} m^2. The effect of the acoustic leak has been largely ignored in past research, but this work shows that the existence of a leak can limit the attenuation of an ear cup by over 50 dB, compared to the ideal no leak scenario below 800 Hz.

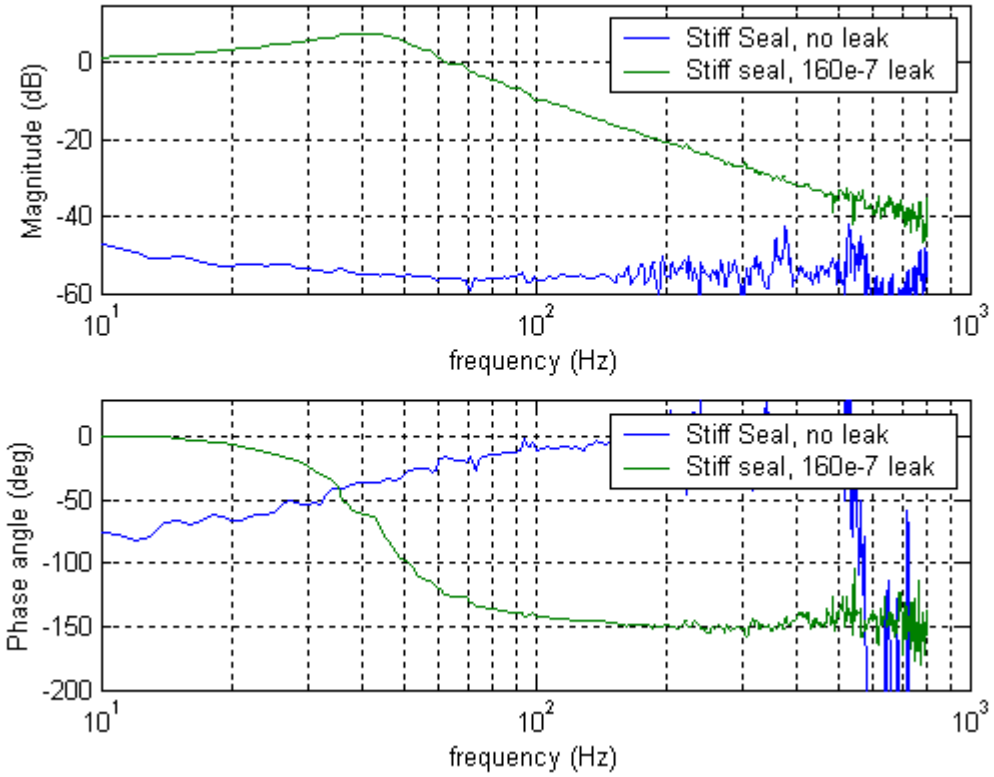

Figure 5.1: Attenuation limit of ear cup

Figure 5.1 (NSAR-1M3-F-NEW, HAR-1M3-F-160) is a comparison of a no leak case, and a case with a leak of 160e^{-7} m^2. This is an example of how much a small leak can affect the low frequency attenuation of an ear cup. If the leak size is increased, the attenuation of the ear cup would degrade further. The comparison in Figure 5.1 is made to the no leak case of the stiff seal. This seal showed the best attenuation results for low

frequencies. A comparison of the data in Figure 5.1 demonstrates the attenuation limits of the ear cup.

The secondary goal of this research was to measure the mid frequency response of the ear cup and look at factors that may affect noise attenuation in this range. This was accomplished by examining the mid frequency mode shapes that occur within the ear cup. Each of these mode shapes correspond to decreased attenuation at their resonant frequency. Successful identification of the first few mode shapes of the ear cup shows that the FE modeling is doing a good job predicting the dynamics of the ear cup.

Finally, the results of the velocity tests show compelling evidence that the effect of leak extends well beyond the Helmholtz resonance. The tests show that the fluid in the leak maintains a constant acceleration with respect to frequency as high as 3000 Hz. This means that the leak continues to be a dominant dynamic up to 3000 Hz, and is no longer a low frequency effect. It also further information to show the leak can no longer be ignored when analyzing the attenuation of a circumaural hearing protector.

5.1 Future Work

Current research has made great strides in modeling and testing the low frequency dynamics of the ear cup. The identification and characterization of the low frequency modes is a first step towards the full understanding of hearing defenders. This document focused on the low frequency dynamics, and briefly investigated the mid-frequency acoustics. The FE analysis of the acoustic modes is a part of the future work to be conducted. FE analysis allows for a three dimensional study of the pressure field within the ear cup. Three-dimensional testing of the mid-frequency pressure field also needs to be conducted in order map out the sound pressures throughout the entire volume of the cup. All of the low frequency Helmholtz tests were conducted with a single leak. An ear cup will have more than one leak, and the leaks will be of varying sizes. The affect that this has on the cup dynamics needs to be examined.

After conducting more tests, the next step is to begin designing an ear cup that will attenuate noise more effectively than currently available ear cups. While there is still much work to be done, the results of this research have led to a new understanding of attenuation in ear cups.

References

1) L.E. Kinsler, A.R. Frey, A.B. Coppens, J.V. Sanders, "Fundamentals of Acoustics", John Wiley & Sons, Inc, New York, 2000.

2) R. Pääkkönen, "Effects of cup, Cushion, Band Force, Foam Lining, and Various Design Parameters on the Attenuation of Earmuffs," Noise Control Engineering Journal, vol. 38, n2, pp 59-65.

3) R. Goff, W. Blank, "Field Evaluation of Muff Type Hearing Protection Devices," Sound and Vibration, vol 18, n10, pp 16-17, 20-22.

4) H.E. von Gierke, D.R. Brown, "Protection of the Ear from Noise: Limiting Factors," BENOX report, Contract N6 ORL-020.

5) T.W. Rimmer, M.J. Ellenbecker, "Feasibility Assessment of a New Method for Measurement of Hearing Protector Attenuation: Bone Conduction Loudness Balance," APPL.OCCUP.ENVIRON.HYG, January 1997, pp 69-75

6) G.J. Thiessen, E.A.G. Shaw, "Ear Defenders for Noise Protection," Aviation Medicine, November 1958, pp 810-814.

7) E.H. Berger, R.W. Kieper, "Hearing Protection: Surpassing the Limits to Attenuation Imposed by the Bone-Conduction Pathways," The Journal of the Acoustical Society of America, Vol 114, n4, pp 1955-1967.

8) G.J. Thiessen, E.A.G. Shaw, "Acoustics of Circumaural Earphones," The Journal of the Acoustical Society of America, Vol 34, September 1962, pp 1233-1246.

9) Y.L. Hsu, C.C. Huang, C.Y. Yo, C.J. Chen, C.M. Lien, “Comfort Evaluation of Hearing Protection,” International Journal of Industrial Ergonomics, Vol 33, 2004 pp. 543-551.

10) R.S. Birch, S.N. Gerges, E.F. Vergara, “Design of a Pulse Generator and Shock Tube for Measuring Hearing Protector Attenuation of High-Amplitude Impulsive Noise,” Applied Acoustics, Vol. 64, 2003, pp. 269-286.

11) W.J. Murphy, E.H. Berger, A. Behar, J.G. Casali, C. Dixon-Ernst, E.F. Krieg, B.T. Mozo, J.D. Royster, L.H. Royster, S.D. Simon, C. Stephenson, “Development of a New Standard Laboratory Protocol for Estimation of the Field Attenuation of Hearing Protection Devices: Sample Size Necessary to Provide Acceptable Reproducibility,” The Journal of the Acoustical Society of America, Vol 115, n1, pp 311-323.

12) F. Fahy, “Sound and Structural Vibration,” Academic Press Inc. , Orlando, 1987.

13) D.A. Bies, C.H. Hansen, “Engineering Noise Control,” Spon Press, New York, 2002.

14) D.J. Ewins, “Modal Testing: Theory and Practice,” Research Studies Press LTD, Letchworth, 1986.

15) J. Borwick, “Loudspeaker and Headphone Handbook,” Focal Press, Oxford, 1998.

Appendix A

Microphone Test Indexing system

HAL-1M1-PS-070

Type of test | Frequency range | Source Location | Signal mic location | Ref mic location | Data and microphone type | Leak size ($x10^{-7}$ m^2)

Type of test:

H	Helmholtz	
N	No leak (there may be a modifier for different seals)	1 = 2.5”
F	Full model dynamics	2 = 2.25”
	Z = duct leak, DCCI undercut seal	3 = 2”
	V = circular leak, DCCI undercut seal	4 = 1.75”
	X = circular leak, grey foam seal	
	Y = duct leak, grey foam seal	
I	Two leaks (equal size Helmholtz)	
	G = Large speaker	
	B = Small speaker	
J	On the head testing (no modifier means no seal)	
	V = DCCI undercut seal	
	G = grey foam seal	
	S = stiff gasket material	
C	Foam cross Helmholtz test	
G	Large foam insert test	

Frequency Range:

A	0-800 Hz
B	0-1600 Hz
C	0-3200 Hz
D	0-6400 Hz
E	0-12.8 kHz
F	0-25.6 kHz

Source Location

L	aimed at the leak
T	aimed at the top of the cup
F	Far Field (diffuse)
C	equidistant from the leak

Signal Microphone Location:

(first character)

#	Cage location (see cage diagram)

(Second character)

B	Bottom (closest to ear)
M	Middle
T	Top (furthest from ear)

Reference Microphone Location:

1	top center of cup
2	mid, long side of cup
3	bottom, long side of cup
4	mid, short side of cup
5	bottom, short side of cup

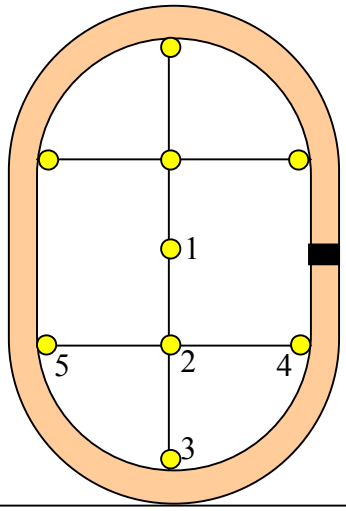

Black area is the leak, and this is looking down from the top

Data and microphone type:

F	Frequency Response (both microphones)
PS or PR	Power spectrum for reference of signal microphone

*All modifiers come after the section letter or number

Appendix B

Experimental and FEA modal results for the ear cup

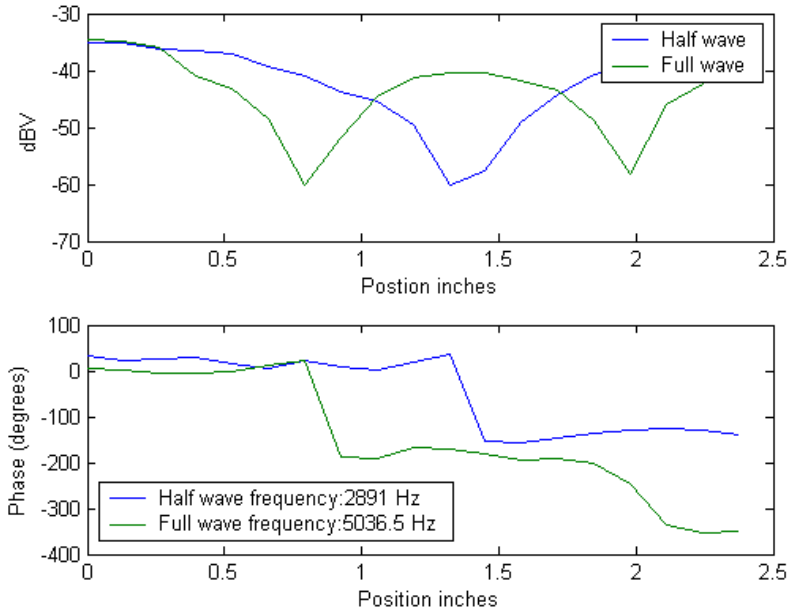

Figure B. 1: Experimental results of standing waves along width axis of cup

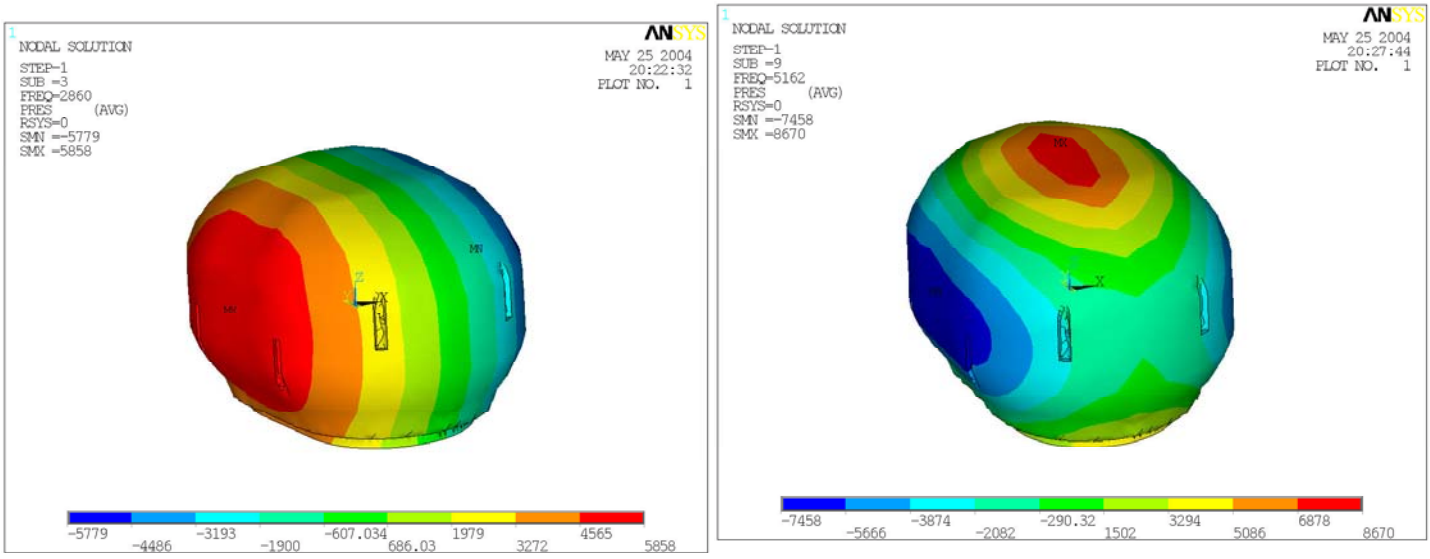

Figure B. 2: Standing half wave along width axis (left) and standing full wave along width axis (right)

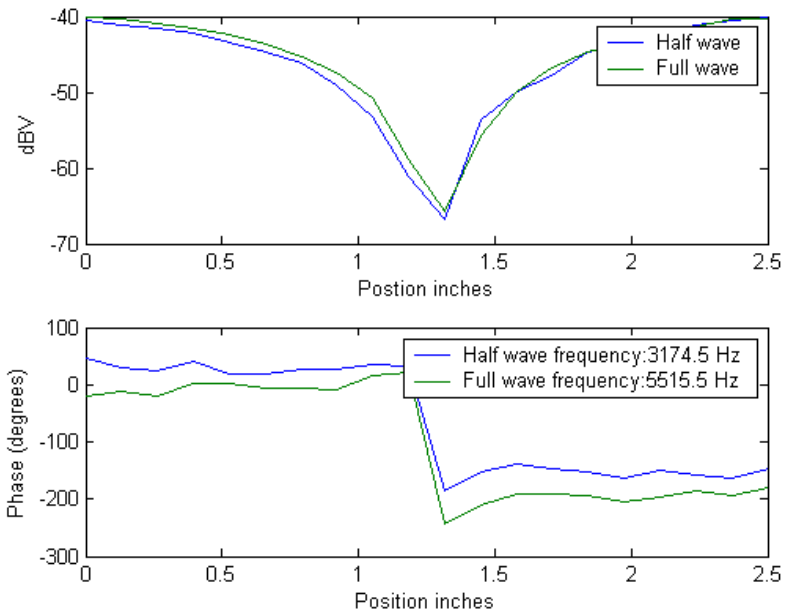

Figure B. 3: Standing waves along height axis of cup

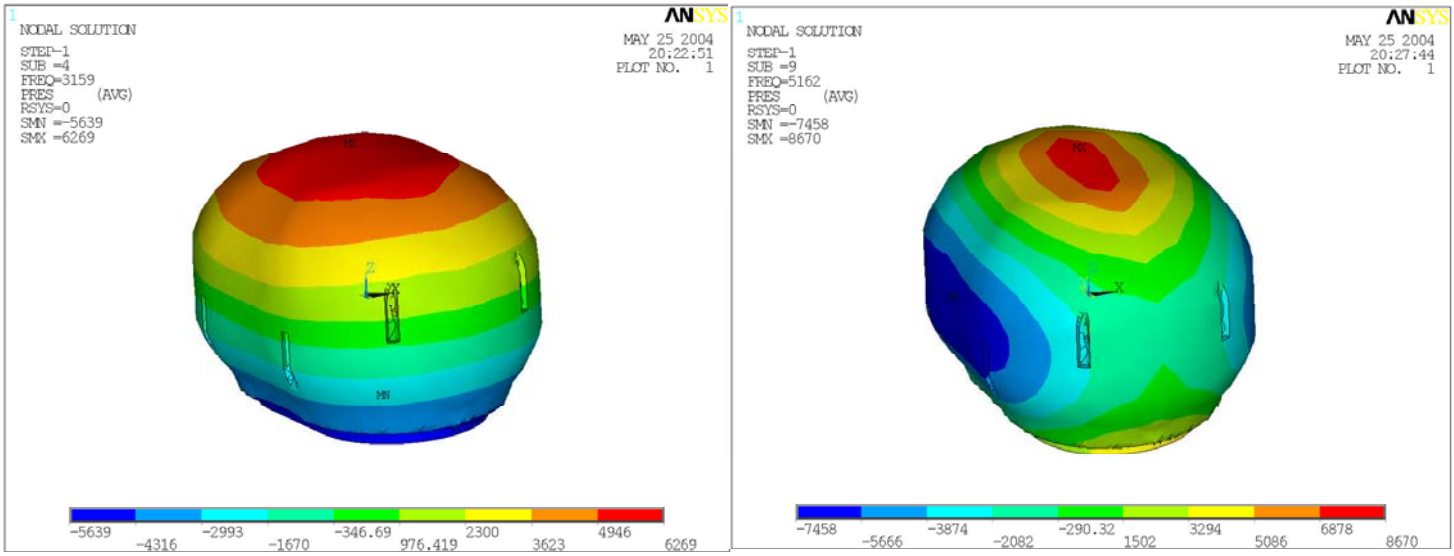

Figure B. 4: Standing half wave along height axis (left) and standing full wave along height axis (right)